Cell Communication and Signaling

RESEARCH Open Access

# Intestinal inflammation and microbiota modulation impact cochlear function: emerging insights in gut-ear axis

Anna Pisani[1†], Valentina Petito[2†], Fabiola Paciello[3,4*], Valeria Emoli[2], Letizia Masi[2], Veronica Mohamed Hizam[5], Pierluigi Puca[2,9,10], Raffaele Montuoro[5], Federica Del Chierico[7], Lorenza Putignani[6], Claudio Grassi[3,4], Jacopo Galli[4,5], Maurizio Taglialatela[1], Maria Emiliana Caristo[8], Gianluca Ianiro[2,9,10], Loris Riccardo Lopetuso[2,9,11], Giovanni Cammarota[9,10], Antonio Gasbarrini[2,9,10], Anna Rita Fetoni[1*†] and Franco Scaldaferri[2,9,10†]

## Abstract

**Background** Although several evidence demonstrates a "gut–microbiota–brain axis", suggesting a bidirectional communication between gut microbiota and the central nervous system, less is known about a possible link between the gut and the peripheral nervous system, including the inner ear.

**Methods** Here, we investigated the impact of intestinal inflammation and the modulation of gut microbiota through fecal microbiota transplantation on hearing sensitivity. Female C57BL/6 mice were assigned to four groups: control (Ctrl), DSS-induced colitis (DSS), FMT from patients with active ulcerative colitis (FMT aUC), and FMT from patients with ulcerative colitis in remission (FMT rUC). Auditory function was evaluated by auditory brainstem responses (ABR). Morphological and molecular analyses on cochlear tissues were performed using immunofluorescence, histological staining, and Western blot to assess inflammation, oxidative stress, and blood-labyrinth barrier integrity. Donor microbiota composition was characterized by 16S rRNA sequencing, and systemic inflammation was evaluated by measuring serum lipopolysaccharide (LPS) levels.

**Results** We found that intestinal dysbiosis is associated with functional, morphological, and molecular alterations in the cochlea, such as increased oxidative stress, inflammation, and altered blood-labyrinth barrier permeability. This leads to macrophage infiltration and immune response activation through the MyD88/NF-κB pathway. Notably, these effects were exacerbated by FMT from subjects with aUC, while FMT from patients with rUC provided a protective effect on cochlear functions.

[†]Anna Pisani and Valentina Petito contributed equally to this work.

[†]Anna Rita Fetoni and Franco Scaldaferri share the senior authorship.

*Correspondence:
Fabiola Paciello
fabiola.paciello@unicatt.it
Anna Rita Fetoni
annarita.fetoni@unina.it

Full list of author information is available at the end of the article

**Conclusions** Overall, our findings suggest that gut inflammation, microbiota alteration, or its therapeutic modulation can impact inner ear pathology: worsening gut inflammatory status negatively affects hearing sensitivity, while the restoration of gut microbiota positively impacts auditory function.

**Plain English summary**

While the gut-brain axis has been widely studied, less is known about the potential connection between gut health and structures of the peripheral nervous system, such as the inner ear. In this study, we examined whether gut inflammation and changes in gut bacteria (microbiota) can impact hearing. We used a mouse model to mimic intestinal inflammation by administering a chemical (DSS) that induces colitis. Some mice also received fecal microbiota transplantation (FMT), a procedure in which gut bacteria from patients with ulcerative colitis (UC) were transferred into the mice. We tested two types of FMT: one from patients with active UC (severe inflammation) and another from patients with quiescent UC. Our results showed that intestinal inflammation negatively affects hearing by causing damage to the inner ear. Mice with colitis exhibited increased inflammation, oxidative stress, and weakening of the blood-labyrinth barrier, a structure that normally protects the ear. Mice that received FMT from patients with active UC experienced even more severe hearing impairment and inner ear damage. Conversely, those that received FMT from patients with quiescent UC showed reduced damage and better hearing, suggesting that a healthier gut microbiota may have a protective effect on the auditory system.

These findings suggest that gut health and microbiota composition can influence hearing. While severe gut dysbiosis worsens cochlear damage, microbiota modulation through FMT may offer protective effects. This highlights the potential of microbiota-based therapies to prevent hearing loss, particularly in individuals with inflammatory bowel disease.

**Keywords** Cochlea, Gut dysbiosis, Gut microbiota, Inflammation

## Introduction

Over the past decade, a growing interest in the field of neuroscience has been focused on the interaction between intestinal microbial communities and the central nervous system (CNS), introducing the concept of the "gut–brain axis" [1, 2]. Several studies demonstrated a bidirectional communication between gut bacteria and brain structures, showing that the gastro-intestinal tract can influence cognitive functions, and vice versa. Furthermore, great efforts have been made to identify the complex network involved in maintaining gastrointestinal and CNS homeostasis, identifying different potential communication pathways between the gut microbiota and the brain [3, 4].

The gut microbiota is considered a metabolic and immune organ, regulating different physiological functions, such as nutrient absorption, metabolism, permeability of the epithelial barrier and modulation of immunity against pathogens [5]. An imbalance in the relationship between gut microbes and the immune system can lead to harmful consequences. On one hand, intestinal bacteria may promote inflammatory responses in other tissues outside the gut, boosting cytokine signaling, as well as reactive oxygen species (ROS) production, and leading to inflammatory-oxidative damage [6, 7]. On the other side, immune cells can trigger inflammatory responses, promoting the secretion of pro-inflammatory agents [8–10], and further increasing the level of oxidative stress in the intestinal tract [11, 12]. Moreover, an imbalance of microbial-immune system interaction results in an increased permeability of the intestinal barrier [13, 14]. Consequently, pathogens can then infiltrate the bloodstream, enabling them to spread to other organs, leading to extraintestinal, sometimes life-threatening, damage [14].

Interestingly, gut-derived oxidative stress and inflammation are considered the main detrimental mechanisms of several neuropsychiatric and neurodegenerative pathologies, either in the central or in the peripheral nervous system. Specifically, mechanisms underlying cochlear damage include increased ROS production, the rise of inflammatory signaling, macrophage infiltration and alteration of the redox balance [15–18].

Considering the similarities between sensory and cognitive neurodegeneration, as well as the functional and structural commonalities between the blood-brain barrier (BBB) and the blood labyrinth-barrier (BLB), the existence of a "gut-inner ear axis" connecting the gut microbiota and the inner ear has been hypothesized [19]. Although sensorineural hearing loss has been speculated to be correlated with gastrointestinal or metabolic pathologies [20–22], to date no data support a possible association between the gut and hearing impairment, and the molecular mechanisms underlying the gut-cochlear axis. This physiopathological substrate could explain the individual variability in susceptibility to cochlear neurodegenerative conditions in such patients with acquired sensorineural hearing loss.

Thus, in this study, we explored the molecular mechanisms underlying the possible association between gut

microbiota alterations and cochlear pathology. Specifically, we used an animal model of dysbiosis, intestinal inflammation (colitis) and altered intestinal permeability induced by dextran sulfate sodium (DSS) administration. Besides, thanks to fecal microbiota transplantation (FMT) from patients with active or inactive ulcerative colitis (UC), we investigated the effect of gut microbiota alterations or repair on cochlear function.

## Materials and methods

### Animals and experimental groups

A total of 67 C57BL/6 female mice eight weeks old were used for the experimental procedures. Mice were divided into 7 experimental groups: (1) "Ctrl" group; $n = 12$; (2) animals receiving a mixture of antibiotics ("ABX" group; $n = 12$); (3) animals receiving ABX and DSS dissolved in tap water as a model of gut dysbiosis ("DSS" group; $n = 11$); (4) animals receiving ABX, DSS and fecal suspension from aUC patients ("FMT aUC" group; $n = 8$); (5) animals receiving ABX, DSS and fecal suspension from rUC patients ("FMT rUC" group; $n = 8$); (6) animals receiving ABX and fecal suspension from aUC patients ("ABX + FMT aUC" group; $n = 5$); and (7) animals receiving ABX and fecal suspension from rUC patients ("ABX + FMT rUC" group; $n = 6$). Moreover, to control the impact of DSS administration on hearing thresholds, $n = 5$ animals receiving only DSS were also used ("DSS-only" group). The antibiotic mixture (400 µl, by gavage) was composed by [23]: Vancomycin (0.125 mg/die; Hikma S.p.A., Pavia, Italy); Amoxicillin (0.25 mg/die; GlaxoSmithKline S.p.A., Verona, Italy); Metronidazole (0.25 mg/die; Alfasigma S.p.A., Bologna, Italy); Gentamicin (0.25 mg/die; Euroclone S.p.A., Pero, Italy) to allow following experiments with FMT (400 µl, by gavage).

To induce acute experimental colitis, mice were administered 3% (w/v) DSS (MP Biomedicals, Aurora, OH, USA) in their drinking water for 7 days following antibiotic treatment, then allowed to recover for a further 7 days. A schematic representation of experimental procedures is shown in Fig. 1. On alternate days body weight, fecal consistency, and the presence of occult fecal blood were monitored in order to calculate the Disease Activity Index, DAI [24]. At sacrifice, 2 ml of whole blood was collected and centrifugated to separate the corpuscular

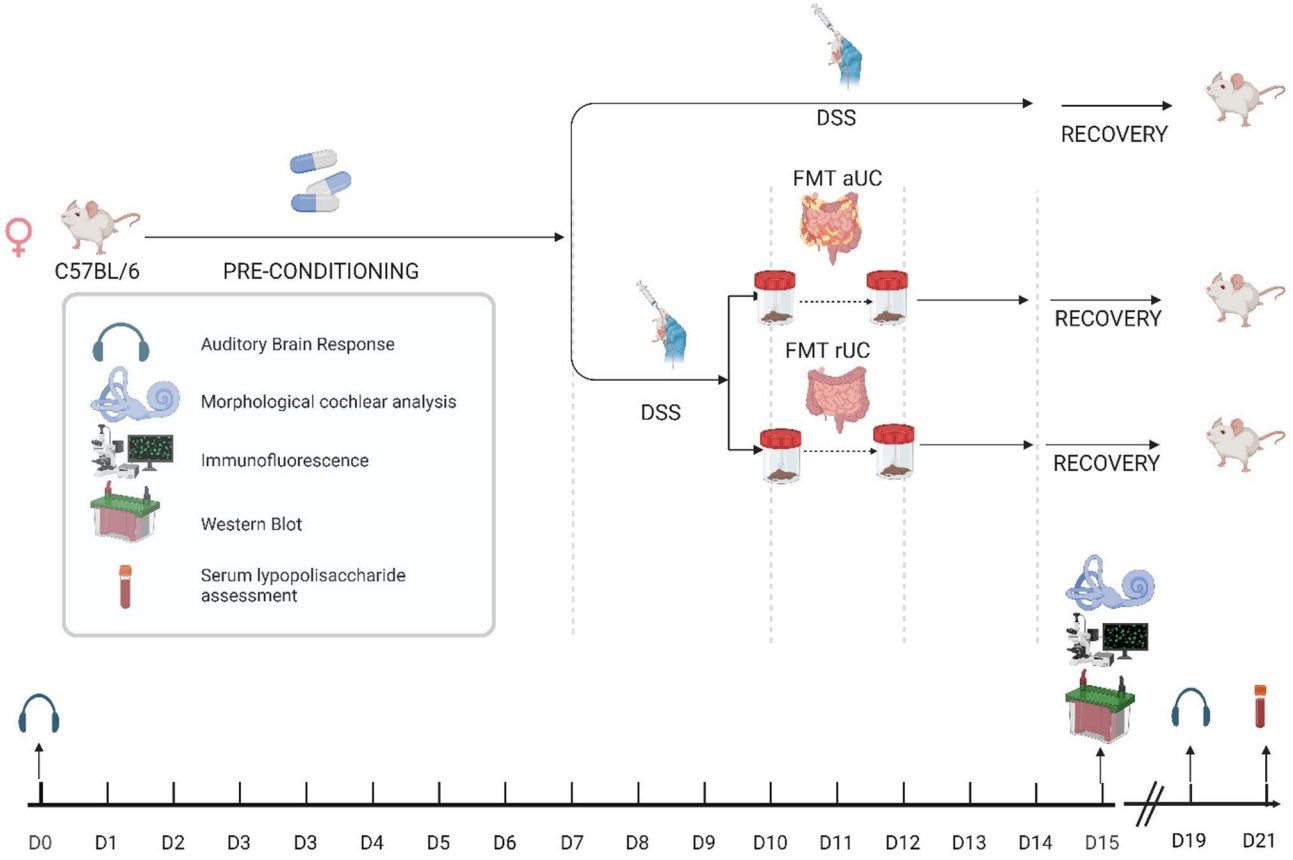


**Fig. 1** Experimental design. C57BL/6 mice of 2 months of age at the beginning of the study were randomly assigned to "Ctrl", "DSS", "FMT rUC" and "FMT aUC" groups. Baseline hearing thresholds were evaluated the day before (D0) the beginning of treatments. Functional (ABR), morphological (immunohistochemistry) and molecular evaluations (Western Blot and immunofluorescence) were performed at the end of treatments. ABR: Auditory Brainstem Responses; FMT: Fecal Microbiota Transplantation. Created by using Biorender Academic Lab License

part from the serum. Animals were maintained with free access to food and water.

#### Fecal microbiota transplantation

During DSS week, after preconditioning with antibiotics, FMT was performed on day 10 and day 12 by oral gavage. The fecal suspension was obtained from 4 g of fecal material from patients with active (aUC) and inactive UC (rUC) being treated at the IBD center within the Center for Diseases of the Digestive System (CEMAD) of the Fondazione Policlinico Universitario "A. Gemelli" IRCCS after administration of informed consent. After a 30-minute homogenization with a lysis solution, fecal buffer water (1% BSA, 50 mM Tris pH 7.5, 0.15 M NaCl), the mixture underwent 3 sequential filtrations of 100 µm, 70 µm and 40 µm to remove large residues and leave the composition of the bacterial population as unaltered as possible. At the end of treatment with 3% DSS and FMT (day 14), the mice had one week of recovery before sacrifice.

#### Patients

Use of human participants in this study was approved by the ethics committee of the Fondazione Policlinico Universitario "A. Gemelli" IRCCS, Rome, Italy (ID 3708/2021) and was conducted in accordance with the Principles of Good Clinical Practice and the Declaration of Helsinki. All participants provided written informed consent to participate in the study. In particular, two patients with active UC and two patients with remission UC were enrolled. Disease activity was assessed according to Partial Mayo Score (PMS) [25]: UC was considered in remission when PMS ≤ 2; active disease was as a PMS between 3 and 5, and moderate-severe disease activity as a PMS greater than 5. Faeces from each patient were equally distributed in the specific treatment group.

#### Donor fecal microbiota profiling

DNA from 200 mg of donor fecal samples was extracted using the QIAamp Fast DNA Stool kit, following the manufacturer's instructions (Qiagen, Germany).

The variable region V3-V4 of the 16S rRNA gene (~460 bp) was amplified and sequenced on an Illumina MiSeqTM platform according to the manufacturer's specifications to generate paired-end reads [26]. Raw reads were filtered for their quality, read length and chimera presence by the QIIME pipeline [27]. Bacterial taxa were obtained by PyNAST v.0.1. program against Greengenes 13_08 database with a 97% similarity for bacterial sequences [28].

#### Detection of LPS levels in serum

Detection of trace amounts of bacterial endotoxin (LPS) in serum was performed using the Limulus Amebocyte Lysate (LAL) kit (Hycult, Uden, The Netherlands). Serum samples and standards were incubated in microtiter wells; the LAL reagent binds to the endotoxin and reacts by developing a yellow color. The enzymatic reaction is stopped after 20 min of incubation by the addition of acetic acid. The absorbance at 405 nm is then measured with a spectrophotometer. A standard curve was generated by plotting the absorbance (linear) against the corresponding concentrations of the endotoxin standards (log); from this curve, the concentration of endotoxin in the samples can be determined.

#### Intestinal cytokine analysis

A part of colon tissues was used to extract the proteins: RIPA buffer (with protease and phosphatase inhibitors, Sigma-Aldrich, Darmstadt, Germany) was added to homogenized on ice the tissues by using a polytron. Sonicated samples were centrifuged at 10,000 rpm at 4 °C for 10 min, and the supernatants were removed and stored at 4 °C prior to the assay of TNF-α, IFN-γ, IL6 and IL33 via ELISA (Multiplex Luminex®Assay, R&D Systems, Minneapolis, MN, US). The assay was performed according to the manufacturer's instructions. Total soluble protein was also determined by using supernatant of sonicated samples via bicinchoninic acid protein assay (Bio-Rad, Hercules, CA, US) and cytokine levels were normalized on total protein amount.

#### Histological observation and scoring

Colon tissue was fixed in 4% formalin, embedded in paraffin and hematoxylin and eosin (HE)-stained sections were scored blindly on the basis of severity and extent of inflammation, as well as presence and extent of ulceration. Scores ranged from 0 to 4 for each parameter; single values were summed up to obtain the overall histological score (maximum possible value equals 16). Photomicrographs were taken with 40 × magnification on a Nikon E400 Eclipse microscope. For accurate quantification of H/E infiltrating in colon tissue, we employed an unbiased stereological technique by means of the Stereo Investigator System (Stereo Investigator software, Version 9.14© 2010, MicroBrightField Europe, Magdeburg, Germany) as previously described. This technique allows quantitative and unbiased evidence of a three-dimensional structure to be obtained, based on the analysis performed on two-dimensional histological sections. The cellular density of cells was determined by dividing the number of cells from three different fields by the area of region of interest (ROI) of colon tissue with the Stereo Investigator software (Version 9.14© 2010, MicroBrightField Europe, Magdeburg, Germany).

#### Measuring auditory function (ABR recordings)

To evaluate auditory function, we measured Auditory Brainstem Responses (ABRs). In all animals, ABRs were evaluated bilaterally at different frequencies (6, 12, 16, 20, 24 and 32 kHz) before and after treatments, as shown in Fig. 1, illustrating our experimental workflow. As previously reported [29], animals were anesthetized (ketamine, 35 mg/kg and medetomidine-domitor, 0.25 mg/kg) and placed in an anechoic room. To record auditory potentials, three stainless steel electrodes were placed subcutaneously into the right mastoid (active), vertex (reference) and left mastoid (ground). Electrophysiological evaluations were performed by using the TDT System 3 (Tucker–Davis Technologies, Alachua, FL, United States), which incorporated real-time digital signal processing. Monaural presentation of tone bursts, spanning from 6 to 32 kHz (1 ms rise/fall time, 10 ms total duration, 20/s repetition rate). The recorded responses were filtered (0.3–3 kHz), digitized, and averaged across more than 500 discrete samples for each frequency and sound level used. Threshold values were determined as the minimum stimulus level (in dB) at which a consistent waveform-based onset could be observed, indicating repeatability.

#### Morphological analyses in the cochlea

Surface preparations to obtain both basilar membrane preparations and *stria vascularis* whole mount were obtained from 5 cochleae/group.

Morphological analyses in the organ of Corti were performed by staining hair cells with F-actin. Surface preparation of the organ of Corti was obtained as previously described [30] and the staining was performed by incubating samples with ActinGreen 488 Ready Probes Reagent. The samples were mounted with ProLongTM mounting medium (details on the antibodies used are reported in Table 1) and a confocal microscope system (Nikon Ti-E, Confocal Head A1 MP, Tokyo, Japan) was used to capture images of the immune-labelled specimens using 20× objective lens.

Longitudinal cochlear cryosections (6 µm thickness) obtained by using a Cryostat (SLEE) were used to evaluate the morphology of SGN and immunofluorescence evaluations by using 5 cochleae/group.

To study histological alterations in the *stria vascularis*, lateral wall and spiral ganglion neurons, we performed Hematoxylin and Eosin staining (H&E Staining Kit, ab245880, Abcam) as previously described [29]. The analyses of *stria vascularis* total area, as well as hair cells, fibrocytes and SGNs count, were performed by using ImageJ 1.43u software.

#### Immunofluorescence analyses

Cochlear samples were extracted and processed as described previously [31] and samples/sections were incubated overnight at 4 °C with primary antibodies including: anti-desmin, anti-IBA-1, anti-$Na^+/K^+$-ATPase α1, anti-GSH, anti-iNOS, anti-NF-κB, anti-IL-1β and anti-occludin. Samples were washed in PBS and incubated at RT for 2 h in the dark with labelled-conjugated donkey anti-rabbit and/or anti-mouse secondary antibodies (Alexa Fluor® 488 or 546, Invitrogen). Samples were counterstained with DAPI for 20 min in the dark at RT and mounted with ProLongTM mounting medium (details on the antibodies used are reported in Table 1).

To evaluate the ROS amount, we used dihydroethidium (DHE) staining as described in [30]. To evaluate the cochlear blood barrier, we isolated the *stria vascularis* from the other cochlear structures as described previously [31] and then, samples were incubated with Alexa Fluor® 546 donkey anti-mouse IgG (ThermoFisher) for 2 h at RT. Images were captured with a confocal microscope system (Nikon Ti-E, Confocal Head A1 MP, Tokyo, Japan) with a 20× objective lens. To validate the reliability of immunofluorescence staining, we performed control experiments by excluding the incubation with the primary antibodies in samples randomly selected (data not shown).

#### Western blot and dot blot

Protein lysates were obtained from 3 to 6 cochleae/group by using the same protocol previously published [31, 32]. For dot blots, lysates (5 µl; 5 µg/µl) were carefully applied onto a nitrocellulose membrane pre-wetted with TBST. We ensured equal protein loading by staining the membrane with Ponceau S. The membranes were processed as described in [32] and then incubated overnight at 4 °C with the following primary antibodies: anti-NF-κB; anti-IL-1β; anti-MyD88; anti-ZO-1; anti-occludin, anti-desmin; anti-3-NT; anti-4-HNE and anti-GSH; anti-iNOS; anti $Na^+/K^+$-ATPase α1 and anti-CD45. After three 10-minute rinses in TBST, the membranes were incubated for 1 h at RT with horseradish peroxidase (HRP)-conjugated mouse or rabbit secondary antibodies. Equal protein loading among the experimental samples was confirmed by re-probing the membranes with an anti-GAPDH antibody. UVItec Cambridge Alliance system was used to obtain quantitative analyses of protein expression. Details on the antibodies used are reported in Table 1.

#### Statistical analyses

All statistical analyses were performed using GraphPad Prism (GraphPad Software). Two-way ANOVA multiple-group comparison was used to compare differences between groups. A p-value of $<0.05$ was considered

**Table 1** List of reagents and antibodies used

| Reagent type | Designation | Source | Identifiers | Additional information | Use |
|---|---|---|---|---|---|
| Antibody | Anti-rabbit IgG AlexaFluor 546 (rabbit polyclonal) | Thermo Fisher Scientific | Cat. No. #A-10,040 | IF (1:400) | Secondary antibody for immunofluorescence analyses |
| Antibody | Anti-rabbit IgG AlexaFluor 488 (rabbit polyclonal) | Thermo Fisher Scientific | Cat. No. #A-21,206 | IF (1:400) | Secondary antibody for immunofluorescence analyses |
| Antibody | Anti-mouse IgG AlexaFluor 546 (mouse polyclonal) | Thermo Fisher Scientific | Cat. No. #A10036 | IF (1:400) | Secondary antibody for immunofluorescence analyses |
| Nuclear Counterstains | DAPI | Thermo Fisher Scientific | Cat. No. D1306 | IF (0.5 mg/mL) | Marker of cell nuclei |
| Antibody | ActinGreen | Thermo Fisher Scientific | Cat. No. R37110 | IF (2 drops/ml) | High affinity of F-actin probe (phalloidin) |
| Antibody | Anti-Occludin (rabbit monoclonal) | Cell Signaling | Cat. No. #91,131 | WB (1:1000) | Marker of occludin (tight junction protein) |
| Antibody | Anti-Iba1/AIF-1 (rabbit monoclonal) | Cell Signaling | Cat. No. #17,198 | IF (1:200) | Marker of macrophages |
| Antibody | Anti-CD45 (rabbit monoclonal) | Cell Signaling | Cat. No. #72,787 | WB (1:1000) | Marker of immune cells |
| Antibody | Anti-iNOS (rabbit polyclonal) | Invitrogen | Cat. No. #PA1-036 | WB (1:1000) | Inflammatory marker (Inducible nitric oxide synthase) |
| Antibody | Anti-IL-1b (rabbit polyclonal) | Santa Cruz | Cat. No. Sc-7884 | WB (1:200) | Inflammatory marker (Interleukin-1b) |
| Antibody | Anti-$Na^+/K^+$-ATPase a1 (mouse monoclonal) | Santa Cruz | Cat. No. Sc-21,712 | WB (1:200), IF (1:50) | Marker of $NA^+/K^+$-ATPase pump |
| Antibody | Anti-Desmin (rabbit polyclonal) | Sigma-Aldrich | Cat. No. #D8281 | WB (1:500), IF (1:50) | Marker of pericytes |
| Antibody | Anti-ZO-1 (rabbit polyclonal) | LSBio | Cat. No. LS-B2129-50 | WB (1:500) | Marker of ZO-1 (tight junction protein) |
| Antibody | Anti-Myd88 (rabbit polyclonal) | Cell Signaling | Cat. No. #3699 | WB (1:1000) | Marker of the adaptor protein Myd88 |
| Antibody | Anti- NF-κB (rabbit monoclonal) | Cell Signaling | Cat. No. #8242 | WB (1:1000) | Inflammatory marker (transcription factors of the nuclear factor κB (NF-κB) |
| Antibody | Anti-Glutathione (mouse monoclonal) | Abcam | Cat. No. ab19534 | WB (1:1000) | Marker of glutathione-protein complexes |
| Antibody | Anti-Nitro tyrosine (rabbit polyclonal) | Sigma-Aldrich | Cat. No. #06-284 | WB (1:1000) | Marker of protein tyrosine nitration |
| Antibody | Anti-4HNE (rabbit polyclonal) | Alpha Diagnostic International | Cat. No. #HNE11-S | WB (1:1000) | Detect the 4-Hydroxy-2-nonenal (HNE), a marker of lipid peroxidation |
| Antibody | Anti-GAPDH (mouse monoclonal) | Abcam | Cat. No. ab8245 | WB (1:5000) | Marker of GAPDH protein (Loading control) |

statistically significant in all analyses performed. The statistical tests used are specified in the main text. Bonferroni's *Post-hoc* was used for multiple comparisons. Data are presented as mean ± SEM.

## Results

### DSS colitis and its modulation from FMT aUC and FMT rUC

The timeline of experiments and procedures are shown in Fig. 1. DSS model of intestinal inflammation was settled, and results were consistent with what was expected. Before proceeding to analyses on auditory function, we verified that mice treated with FMT from patients with active UC ("FMT aUC" group) had more severe colitis than mice treated with FMT from patients with UC in remission ("FMT rUC" group), as evidenced by a higher DAI score (Fig. 2A).

The intestinal inflammation was also evaluated by serum LPS levels, and by mucosal pro-inflammatory cytokines, such as TNF-α, IFN-γ, IL6 and IL33, finding the highest levels in DSS group and with levels in FMT aUC mice higher than FMT rUC mice (Fig. 2B-C).

Histologic score, assessed using by Rachmilewitz score, strongly confirms the presence of extensive areas of inflammation in DSS and FMT aUC group (Fig. 2D). Due to the structural complexity of samples studied and to ensure rigorous and unbiased quantitative estimation of data generated by H/E, we turned to the stereological analysis. This analysis demonstrated that the cell density (cells/$mm^2$) was higher in DSS than in control

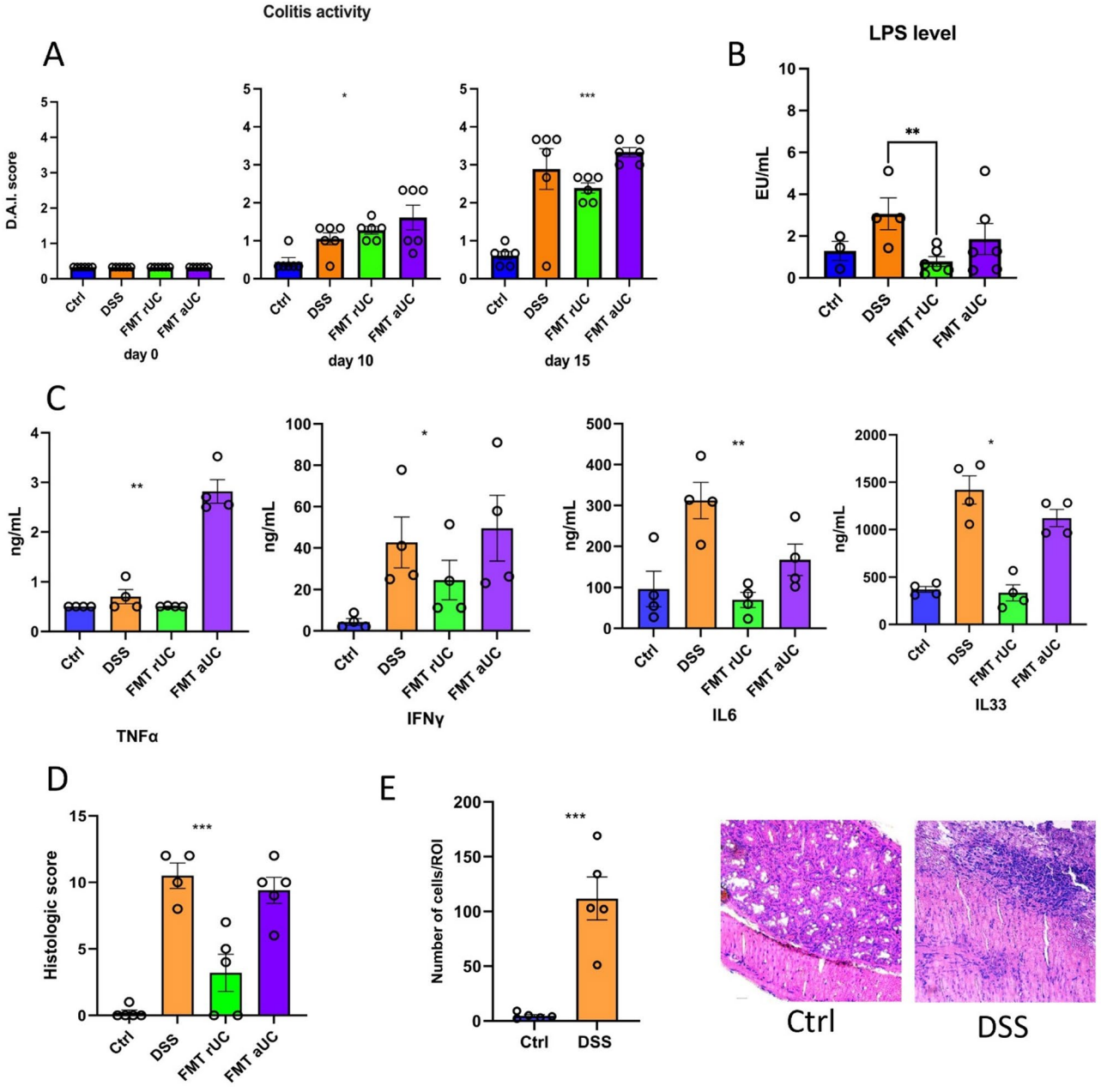


**Fig. 2** Characterization of intestinal inflammation. **A**: Average Disease Activity Index (D.A.I.) on day 15, calculated by assessing weight, fecal consistency, body weight and the presence of occult fecal blood. **B**: Average LPS serum levels in "DSS", "FMT rUC" and "FMT aUC" groups. LPS: Lipopolysaccharide. **C**: Concentration of pro-inflammatory cytokines in intestinal mucosa on day 15. **D**: Histological analysis was performed according to Rachmilewitz score. **E**: Stereological analysis of cell density in both DSS tissue vs. control, from 5 different colon mice. Cell density was determined by dividing cell counts by the area of the ROI. Bars show the mean of cell counts ± standard deviation (left panel). H/E staining of colon tissues from control mice (Ctrl) or treated with DSS (DSS). Magnification 40× (right panel) $*p = 0.05$;$**p < 0.01$; $***p < 0.001$

tissue ($p < 0.001$, Fig. 2E). Our data are consistent with the expression of H/E cells in DSS tissue with a higher cell density revealed in the same region of interest. We also confirmed, through microbiota analysis, a more pronounced dysbiosis in the donor patients affected by active UC in comparison to donors with inactive UC (Fig. 3A).

**Altered microbiota affects auditory function**

To establish a link between gut dysbiosis, altered gut permeability, and altered hearing sensitivity, we recorded ABRs.

No significant differences in the auditory function were observed by comparing the Ctrl vs. ABX group (Fig. 4A), indicating that notwithstanding ABX cocktail pre-treatment, the dosage used had no direct ototoxic effect.

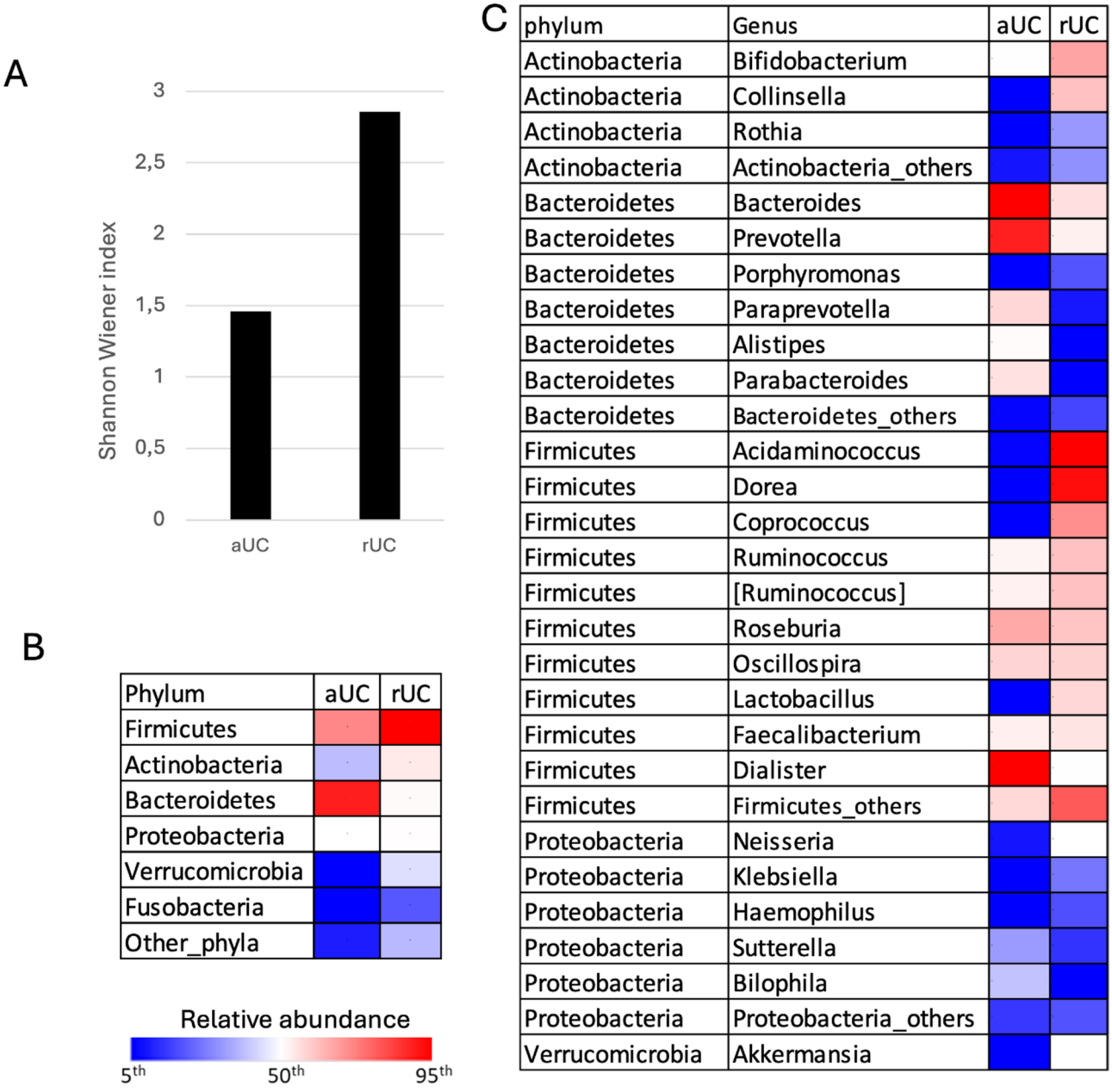


**Fig. 3** Ecological analysis of the gut microbiota of the two donors. **A**: α-diversity index (Shannnon Weiner index) of the two donors: one with active UC (aUC) and the other with UC in remission (rUC). **B**: Heatmap of the relative abundance of the major phyla of gut microbiota from the donor aUC and the donor rUC. **C**: Heatmap of the relative abundance of the major genera of gut microbiota from the donor aUC and the donor rUC

Moreover, no significant differences were observed by comparing auditory thresholds in Ctrl and in animals receiving only DSS (Fig. S1A). Interestingly, no significant differences were observed comparing auditory thresholds of ABX + FMT rUC and Ctrl groups, whereas a significant increase of hearing thresholds (of about 10–15 dB) was found in ABX + FMT aUC animals with respect to controls (Fig. S1B), indicating a detrimental effect of FMT aUC on hearing sensitivity. A slight increase in auditory thresholds (of about 15–20 dB) was observed in DSS group compared to untreated mice, specifically in mid-high frequency (Fig. 4B; two-way ANOVA, 20 kHz $p = 0.0117$; 24 kHz $p = 0.0261$; 32 kHz $p = 0.0037$).

Interestingly, the further modulation of gut dysbiosis and intestinal increased permeability induced by FMT aUC had a more pronounced effect on ear function. Indeed, FMT from aUC donors was associated with a greater elevation of auditory thresholds (of about 20–25 dB), spanning from 12 to 32 kHz compared with baseline values (Fig. 4B; two-way ANOVA, 12 kHz $p = 0.0187$;

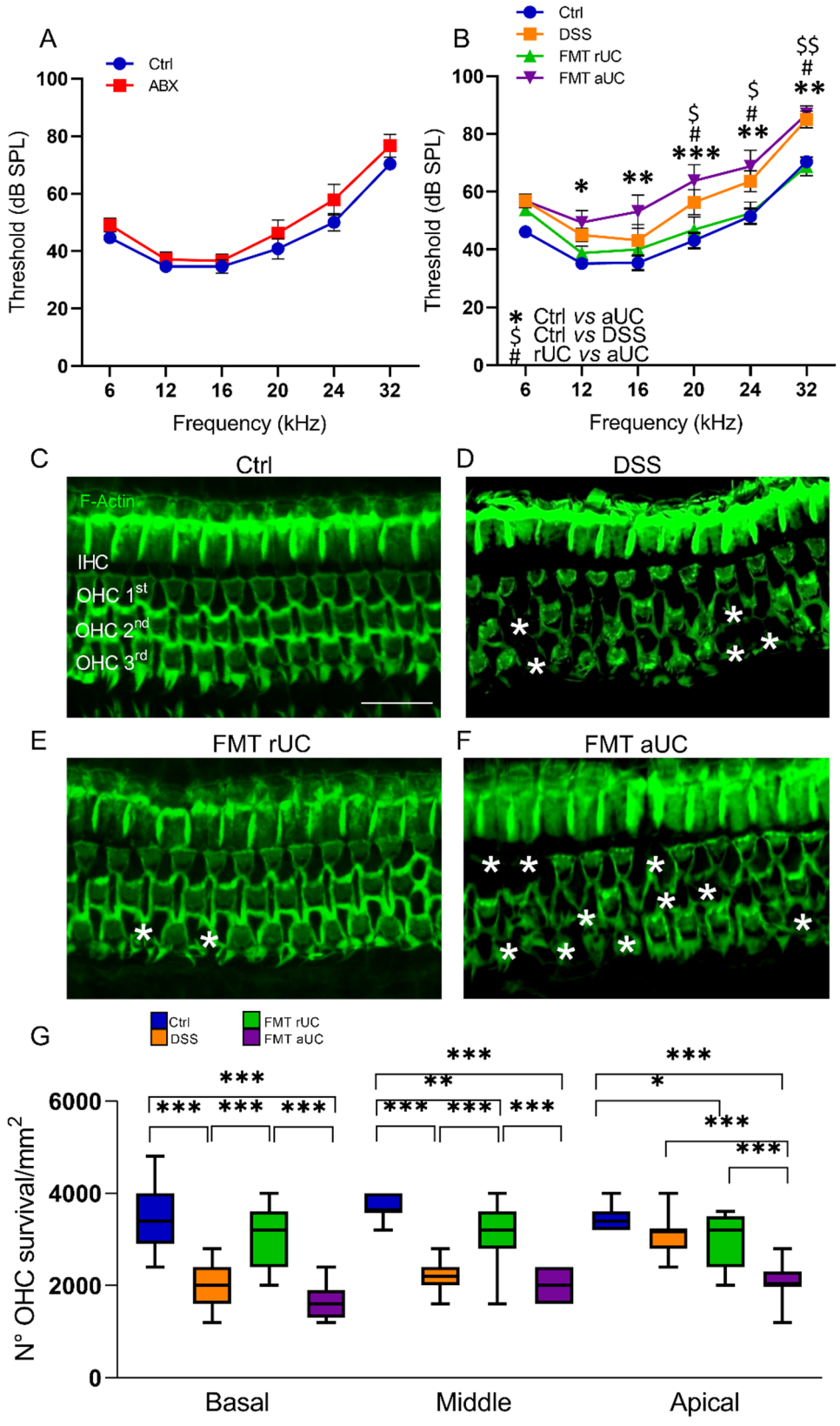


**Fig. 4** (See legend on next page.)

(See figure on previous page.)

**Fig. 4** Functional analysis and morphological evaluations in the organ of Corti: hair cell loss. **A**, **B**: Graphs showing ABR threshold values (means ± SEM) across all frequencies analyzed. **A**: Treatment with ABX alone does not significantly affect auditory thresholds compared to the Ctrl group. **B**: DSS treatment leads to a slight but significant increase of threshold values of approximately 15 dB in the mid-high frequencies (20–32 kHz) compared to the Ctrl group. FMT aUC further increases the auditory threshold of about 20–25 dB, in almost all frequencies analysed, while the FMT rUC group shows a recovery of hearing function. Symbols indicate significant differences among groups ($#*$p < 0.05$; $$** $p < 0.01$; ***$p < 0.001$). **C-F**: Representative images of surface preparations of the organ of Corti in the middle cochlear turn, hair cell distribution labeled with F-actin (green fluorescence). **G**: Cochleograms (means ± SEM) showing the percentage of outer hair cell (OHC) survival in all cochlear turns. Scale bar: 25 µm. Asterisks indicate significant differences among groups (*$p < 0.05$; ** $p < 0.01$; ***$p < 0.001$)

16 kHz $p = 0.0014$; 20 kHz $p = 0.0001$; 24 kHz $p = 0.002$; 32 kHz $p = 0.0036$), demonstrating that exacerbating dysbiosis and inflammatory disease status can consequently worsening hearing, thus confirming its impact on auditory function. On the other side, animals receiving FMT from donors with rUC showed a lower alteration of auditory thresholds compared to FMT aUC mice, specifically in the mid-high frequency region (Fig. 4B; two-way ANOVA, 20 kHz $p = 0.0277$; 24 kHz $p = 0.0381$; 32 kHz $p = 0.0142$) and hearing sensitivity was not significantly different with respect to control mice (Fig. 4B; two-way ANOVA, $p > 0.05$).

These results indicate that a worsening gut inflammatory status, such as in FMT aUC, negatively affects hearing sensitivity, while the restoration of gut microbiota with FMT rUC positively impacts auditory function.

#### Gut dysbiosis is associated with morphological damage in cochlear structures

To examine in depth the cochlear damage associated with altered gut microbiota, we performed a series of morphological analyses, focusing on the principal cochlear structures: the organ of Corti, the spiral ganglion neurons (SGNs) and the lateral wall, including the *stria vascularis* and the spiral ligament.

Our analyses on surface preparations of the organ of Corti showed OHC damage in the DSS group (Fig. 4D) compared to controls (Fig. 4C), and we found hair bundle disorganization, phalangeal scars and dark spots (indicating missing cells), specifically in the middle-basal turn and in the third and second rows of OHCs. No significant differences were observed in the IHC number (data not shown). This morphological damage worsened in animals of the FMT aUC group (Fig. 4F), showing moderate OHC damage in all cell rows and all cochlear turns, whereas a partial recovery to control values was observed in FMT rUC specimens, where lower OHC loss was found (Fig. 4E). Hair cell count in the basal, middle and apical turns of the cochlea confirmed the correlation between intestinal inflammation, FMT and cochlear function. Indeed, in the basal turn, treatment with DSS affects OHC survival with respect to control condition (Fig. 4G, one way ANOVA, Ctrl vs. DSS $p < 0.0001$), but a recovery of OHC survival was observed in FMT rUC animals (Fig. 4G, one way ANOVA, FMT rUC vs. DSS $p < 0.0001$). On the other hand, animals underwent FMT aUC showed a low percentage of OHC survival compared with the other experimental groups (Fig. 4G, one way ANOVA, Ctrl vs. FMT aUC, and FMT rUC vs. FMT aUC: $p < 0.0001$). In the middle turn, similar results were observed (Fig. 4G, one way ANOVA, Ctrl vs. DSS, Ctrl vs. FMT aUC, DSS vs. FMT rUC and FMT rUC vs. FMT aUC: $p < 0.0001$; Ctrl vs. FMT rUC: $p = 0.0015$). In the apical turn, no significant effect of DSS was observed (Fig. 4G, one way ANOVA, Ctrl vs. DSS $p = 0.1223$), but a detrimental impact of FMT aUC was detected (Fig. 4G, one way ANOVA, Ctrl vs. FMT aUC; DSS vs. FMT aUC and FMT rUC vs. FMT aUC $p < 0.0001$).

We also analyzed other cochlear structures including SGNs, *stria vascularis* and lateral wall, focusing on fibrocytes type II, due to their crucial involvement in ion homeostasis, immune response and regulating blood flow (Fig. S2 A). In line with what was observed in the sensory epithelium, we found a decrease in SGN number (Fig. S2 B-E). Specifically, the deleterious impact of DSS on primary afferent neurons was more evident in the basal and middle cochlear turns (Fig. S2 F-G; one way ANOVA, basal turn: Ctrl vs. DSS $p < 0.0001$; middle turn: Ctrl vs. DSS $p = 0.0015$; apical turn: Ctrl vs. DSS $p = 0.0787$). The FMT aUC group showed a lower number of neurons in all cochlear turns, compared to all the other experimental groups (Fig. S2 F-H; one way ANOVA, basal turn: FMT aUC vs. DSS; FMT aUC vs. Ctrl and FMT aUC vs. FMT rUC $p < 0.0001$; middle turn: FMT aUC vs. DSS; FMT aUC vs. Ctrl and FMT aUC vs. FMT rUC $p < 0.0001$; apical turn: FMT aUC vs. DSS; FMT aUC vs. Ctrl and FMT aUC vs. FMT rUC $p < 0.0001$). On the other end, FMT rUC does not worsen the neurotoxic effect of DSS treatment (Fig. S2 F-H; one way ANOVA, basal turn: FMT rUC vs. DSS $p = 0.0005$, FMT rUC vs. Ctrl $p = 0.6309$; FMT rUC vs. FMT aUC $p < 0.0001$; middle turn: FMT rUC vs. DSS $p > 0.999$, FMT rUC vs. Ctrl $p = 0.0248$; FMT aUC vs. FMT rUC $p < 0.0001$; apical turn: FMT rUC vs. DSS $p > 0.999$, FMT rUC vs. Ctrl $p = 0.1616$; FMT aUC vs. FMT rUC $p < 0.0001$).

By evaluating *stria vascularis* morphology (Fig. S2 I-L), we found a more pronounced effect of DSS, significantly affecting *stria vascularis* area only in the basal turn (Fig. S2 M-O; one way ANOVA, basal turn: Ctrl vs. DSS $p = 0.018$; middle turn: Ctrl vs. DSS $p > 0.999$; apical turn: Ctrl vs. DSS $p > 0.999$), whereas a deleterious effect of FMT aUC was observed in all cochlear turns (Fig. S2

M-O; one way ANOVA, basal turn: FMT aUC vs. DSS; FMT aUC vs. Ctrl and FMT aUC vs. FMT rUC $p < 0.0001$; middle turn: FMT aUC vs. DSS; FMT aUC vs. Ctrl and FMT aUC vs. FMT rUC $p < 0.0001$; apical turn: FMT aUC vs. DSS $p = 0.0029$, FMT aUC vs. Ctrl $p = 0.0001$; FMT aUC vs. FMT rUC $p = 0.0016$). Finally, the density of type II fibrocytes (Fig. S2 P-R) confirm the negative impact of DSS on cochlear structures, with a decreased number of fibrocytes observed in the basal and middle turn (basal turn: Ctrl vs. DSS $p < 0.0001$; middle turn: Ctrl vs. DSS $p = 0.0037$; apical turn: Ctrl vs. DSS $p > 0.999$). Once again, FMT aUC worsens this damage, affecting fibrocyte number in all cochlear turns (Fig. S2 P-R one way ANOVA, basal turn: FMT rUC vs. DSS $p < 0.0001$, FMT rUC vs. Ctrl $p > 0.999$; FMT rUC vs. FMT aUC p $p < 0.0001$; middle turn: FMT rUC vs. DSS $p = 0.3156$, FMT rUC vs. Ctrl $p = 0.6324$; FMT aUC vs. FMT rUC $p = 0.0121$; apical turn: FMT rUC vs. DSS $p > 0.999$, FMT rUC vs. Ctrl $p > 0.999$; FMT aUC vs. FMT rUC $p = 0.0154$).

Collectively, our morphological analyses support functional data, indicating that the slight cochlear damage induced by DSS administration can be exacerbated by the adjuvant FMT aUC, thus indicating that microbiota alterations can impact cochlear structures.

### Cochlear damage is due to increased oxidative stress, redox imbalance, inflammation and macrophage activation

Along with the histological and morphological alterations found in the principal cochlear structures, we also observed signs of oxidative stress and redox imbalance, depending on the altered gut microbiome balance. Indeed, the DHE assay revealed a strong rise in ROS amount in cochlear cryosections of DSS mice, compared to control animals (Fig. 5A, B).

Interestingly, we found a decreased red fluorescence in the FMT rUC group, specifically in the organ of Corti and in the *stria vascularis* (Fig. 5C), whereas ROS amount in SGNs seems to be similar comparing DSS and FMT rUC samples (compare panels B and C in Fig. 5). Notably, ROS amount in the cochlear neuronal compartment of FMT aUC samples seems to be higher with respect to DSS treated mice (Fig. 5D), and it was also evident compared to Ctrl group (Fig. 5A). Supporting these data, our dot blot analyses revealed a higher level of protein tyrosine nitration (3-NT; Fig. 5E, I), along with high lipid peroxidation (4-HNE; Fig. 5F, J) in the DSS vs. Ctrl groups (3-NT: $n = 6$ cochleae/group, one-way ANOVA, $p = 0.0057$; 4-HNE: $n = 6$ cochleae/group, one-way ANOVA, $p = 0.0075$). No significant differences were found in the FMT rUC group compared to the DSS group (Fig. 5E, I; 3-NT: $n = 6$ cochleae/group, one-way ANOVA, $p > 0.05$; Fig. 5F, J; 4-HNE: $n = 6$ cochleae/group, one-way ANOVA, $p > 0.05$), whereas higher values were observed in the FMT aUC group (Fig. 5E, I; $n = 6$ cochleae/group, one-way ANOVA, Ctrl vs. FMT aUC $p < 0.0001$; DSS vs. FMT aUC $p = 0.0114$; FMT rUC vs. FMT aUC $p = 0.0003$). We further evaluated the levels of nitric oxide (NO) production by analyzing inducible NOS (iNOS) amounts. Our western blot data show a marked iNOS increase in DSS and FMT aUC groups with respect to control values (Fig. 5H, L; $n = 4$ cochleae/group, one-way ANOVA, Ctrl vs. DSS $p < 0.0001$; Ctrl vs. FMT aUC, $p < 0.0001$; DSS vs. FMT aUC $p = 0.0451$). A significant decrease in iNOS was observed in FMT rUC compared to FMT aUC samples (Fig. 5H, L; $n = 4$ cochleae/group, one-way ANOVA, $p < 0.0001$). The western blot results were confirmed by immunofluorescence analysis, showing marked iNOS fluorescence signal in both DSS and FMT aUC group (Fig. 5N, P), compared to what observed in Ctrl and FMT rUC (Fig. 5M, O).

To investigate redox imbalance, we also evaluated the other face of the coin by studying the endogenous antioxidant system, focusing on protein glutathionylation. Indeed, glutathionylation is a mechanism through which protein functions can be regulated by the redox status, and it can be considered an indicator of oxidized glutathione (GSSG)/reduced glutathione (GSH) ratio, reflexing tissue redox balance. Our results indicate a significant decrease of glutathionylated proteins in the cochlea of DSS animals compared to controls (Fig. 5G, K; $n = 6$ cochleae/group; one way ANOVA, $p < 0.0001$) and the level of glutathionylated proteins was further affected by FMT aUC treatment (Fig. 5G, K; $n = 6$ cochleae/group; one way ANOVA, $p = 0.0182$) indicating additional detrimental effect mediated by FMT from aUC donors. GSH was also markedly increased in FMT rUC with respect to FMT aUC group (Fig. 5G, K; $n = 6$ cochleae/group; one way ANOVA, $p = 0.0002$), suggesting that reestablishing microbiota balance can exert a protective effect against cochlear oxidative stress. Data were also confirmed by immunofluorescence analysis, with a basal level of GSH expression in all cochlear structures in Ctrl specimens (Fig. 5Q), that was significantly reduced in both DSS and FMT aUC groups (Fig. 5R, T). No differences were observed comparing GSH fluorescence between Ctrl and FMT rUC cochlear cryosections (Fig. 5Q, S).

Collectively, these data demonstrate that colitis-associated dysbiosis induces oxidative stress in the cochlea and that reverting microbiota composition by FMT rUC exerts otoprotective effects.

### Cochlear damage is associated with NF-κB and MyD88 activation

Considering that the crosstalk between oxidative stress and inflammation has been recently thought to be one of the crucial pathological mechanisms involved in sensorineural hearing loss in several models, we also studied

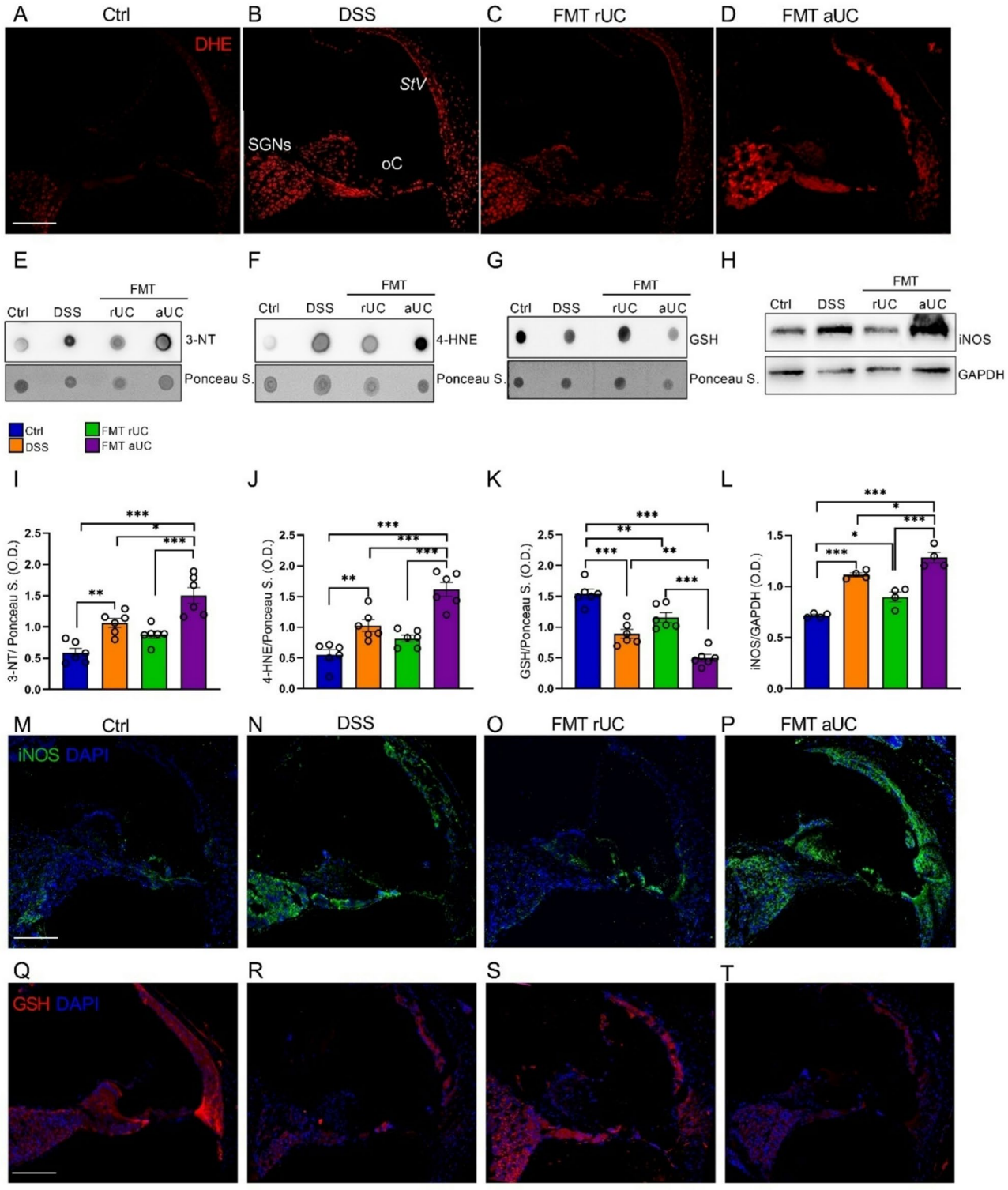


**Fig. 5** Cochlear oxidative stress and redox imbalance associated with gut dysbiosis. **A-D**: Representative images of cochlear cryosections stained with DHE (red fluorescence) to detect ROS amount. Scale bar: 100 µm. **E-G**: Representative dot blot images showing 3-NT (**E**), 4-HNE (**F**) and GSH (**G**) levels in all experimental groups. **I-K**: Histograms (means ± SEM) showing the results of the densitometric analyses normalized to Ponceau S. **H**, **L**: Representative images of iNOS western blot bands (**H**) with the results (means ± SEM) of the densitometric analysis (**L**). **M-T**: Representative images of cochlear cryosections showing iNOS (**M**-**P**, green fluorescence) and GSH (**Q**-**T**, red fluorescence) expression in the principal cochlear structures, in all experimental groups. DAPI staining indicates cell nuclei. Scale bar: 100 µm. Asterisks indicate significant differences among groups (*$p < 0.05$; **$p < 0.01$; ***$p < 0.001$)

inflammatory markers. Specifically, we focused on NF-κB and IL-1β, which are well-known inflammatory agents playing a key role in several diseases [15].

Our western blots showed a marked increased level of NF-κB in the DSS group, compared to controls (Fig. 6A, C; $n = 4$ cochleae/group; one-way ANOVA, $p = 0.0277$) as well as in FMT aUC group, compared with the FMT rUC and Ctrl group (Fig. 6A, C; $n = 4$ cochleae/group; one-way ANOVA, Ctrl vs. FMT aUC $p = 0.0006$; FMT rUC vs. FMT aUC, $p = 0.0033$).

We also found increased levels of the inflammatory marker IL-1β in the same samples (Fig. 6B, E; $n = 4$ cochleae/group; one-way ANOVA, Ctrl vs. DSS $p = 0.0483$; Ctrl vs. FMT aUC $p = 0.0009$; FMT rUC vs. FMT aUC, $p = 0.0098$), indicating that our model of gut inflammatory status was associated with cochlear inflammation. Notably, our immunofluorescence analyses

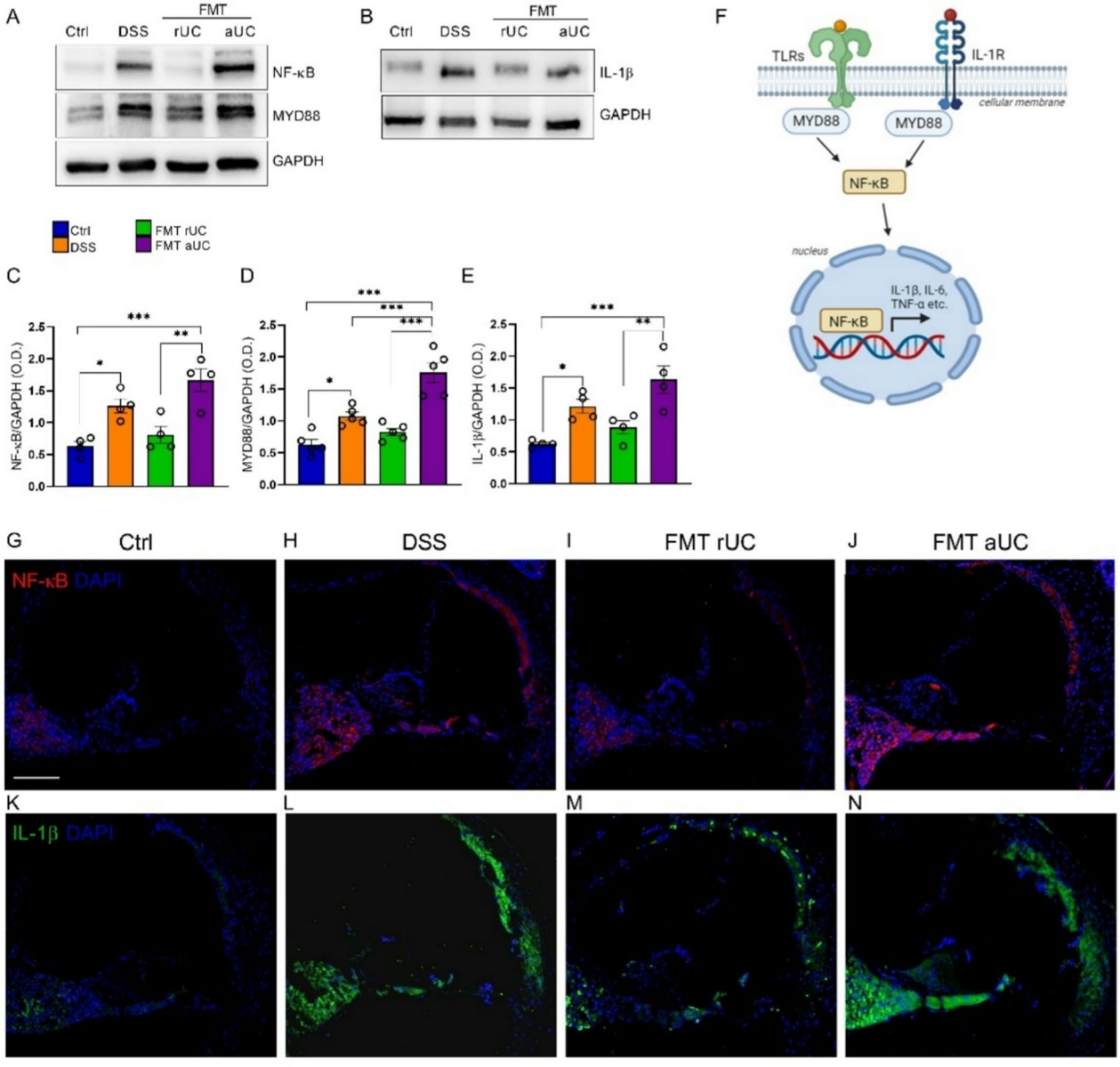


**Fig. 6** Cochlear damage associated with gut microbiota alteration involves inflammation through MyD88/NF-kB pathway. **A**, **B**: Representative western blot images showing the expression of NF-κB, MyD88 (**A**) and IL-1β (**B**) in all experimental groups. **C-E**: Bar graphs showing the results of densitometric analyses for NF-κB (**C**), MyD88 (**D**) and IL-1β (**E**), normalized to total protein level (GAPDH). **F**: Schematic representation of MyD88/NF-κB/ IL-1 pathway. Created by using Biorender Academic Lab License. **G-N**: Representative images of cochlear cryosections showing NF-B (**G**-**J**, red fluorescence) and IL-1β (**K**-**N**, green fluorescence) expression in the principal cochlear structures, in all experimental groups. DAPI staining indicates cell nuclei. Scale bar: 100 µm. Data are expressed as mean ± SEM. Asterisks indicate significant differences among groups (*$p < 0.05$; ** $p < 0.01$; *** $p < 0.001$)

confirmed an increase of both NF-κB and IL-1β in the SGNs, organ of Corti and *stria vascularis* of DSS group, compared to control (Fig. 6G-H and K-L). Similarly, a high NF-κB and IL-1 labeling was found in cochlear cryosections collected from FMT rUC groups, whereas a decreased fluorescence signal was observed in FMT aUC specimens (Fig. 6I-J, M-N).

To gain more insight into the role of the innate immune response, we also evaluated MyD88 protein levels. Indeed, MyD88 is a downstream adaptor protein of toll-like receptors (TLR), a family of receptors involved in pathogen recognition and host defense. When TLRs recognize pathogens, MyD88 is responsible for a cascade of molecular events leading to the activation of the inflammatory response (i.e., NF-κB activation and translocation into the nucleus). Consistently, our western blot data showed a trend of MyD88 protein level similar to what observed for NF-κB and IL-1β, with a significant increase in DSS group with respect to controls (Fig. 6A, D; $n = 5$ cochleae/group; one-way ANOVA $p = 0.0323$), a further enhancement in FMT aUC group (Fig. 6A, D; $n = 5$ cochleae/group; one-way ANOVA, Ctrl vs. FMT aUC $p < 0.0001$; DSS vs. FMT aUC $p = 0.0008$) and a significant reduction in FMT rUC, returning to control levels (Fig. 6A, D; $n = 5$ cochleae/group; one-way ANOVA, Ctrl vs. FMT rUC $p > 0.05$; FMT aUC vs. FMT rUC $p < 0.0001$). These data indicate that gut dysbiosis can trigger the immune response in the cochlea, whereas positively modulating the gut microbiome with FMT rUC can reduce cochlear signs of inflammation.

To further sustain our hypothesis of cochlear inflammation caused by immune system activation, we performed immunofluorescence and western blot analyses to determine macrophage activation and infiltrating leukocytes by using antibodies against IBA-1 and CD45.

Regarding IBA-1, our immunofluorescence analysis in *stria vascularis* whole mounts revealed an increase of IBA-1 positive cells in DSS and FMT aUC groups with respect to Ctrl and FMT rUC groups (Fig. 7A-D, G; one way ANOVA, Ctrl vs. DSS $p < 0.0001$; Ctrl vs. FMT aUC $p < 0.0001$; DSS vs. rUC $p = 0.0175$; FMT rUC vs. FMT aUC $p = 0.0002$).

Moreover, our western blot data indicate an increase of CD45 in DSS cochleae compared to Ctrl (Fig. 7H, I; $n = 5$ cochleae/group; one way ANOVA, $p < 0.0001$) and in FMT aUC compared to FMT rUC samples (Fig. 7H, I; $n = 5$ cochleae/group; one way ANOVA, $p = 0.0005$).

Collectively, our results indicate that the immune system activation is associated with the inflammatory signaling cascade in the cochlea, probably through the MyD88-NF-κB pathway.

#### Gut dysbiosis and gut microbiota alteration affect blood-labyrinth barrier permeability and vascular integrity

To establish a mechanistic connection between our model of intestinal disease, microbiota alterations and cochlear damage caused by oxidative stress, inflammation, and immune cell infiltration, we focused on the blood-labyrinth-barrier (BLB), a semipermeable capillary network controlling exchanges between the blood and the intrastrial space. Thus, we performed western blot analyses to investigate tight junctions (TJs), a class of proteins including ZO-1, claudins and occludins, involved in paracellular permeability. Specifically, we used ZO-1 and occludin as markers of cell-cell junctions in cochlear specimens. By studying ZO-1 we found a significant decrease of protein levels in DSS and FMT aUC groups compared to FMT rUC and Ctrl groups (Fig. 8A, C; $n = 3$ cochleae/group; one way ANOVA, Ctrl vs. DSS $p = 0.0139$; FMT aUC vs. FMT rUC $p = 0.0257$; FMT aUC vs. Ctrl $p = 0.0007$).

By evaluating occludin, we found a significant decrease of protein levels in DSS groups compared to control values (Fig. 8B, D; $n = 4$ cochleae/group; one way ANOVA, $p = 0.0019$) and a decreased level in FMT aUC compared to FMT rUC samples (Fig. 8B, D; $n = 4$ cochleae/group; one way ANOVA, $p = 0.0116$). Results of WB analyses were also confirmed by immunofluorescence analyses showing decreasing occluding label in marginal cell monolayer of *stria vascularis* explants in DSS and FMT aUC groups (Fig. 8F, H), compared to both Ctrl and FMT rUC groups (Fig. 8E, G). These data indicate an alteration of BLB permeability, probably responsible for the cascade of molecular events leading to macrophage infiltration and oxidative/inflammatory cochlear damage. We also focused on $Na^+/K^+$-ATPase α1 expression level, an abundant protein in the BLB playing an essential role in the barrier integrity. Immunofluorescence experiments in cochlear cryosections showing the lateral wall with the *stria vascularis* revealed a strong decreased $Na^+/K^+$-ATPase α1 labeling in DSS and FMT aUC groups, compared with Ctrl and FMT rUC groups (Fig. 8I-L). Western blot performed on total cochlear lysates confirmed these data (Fig. 8M, N; $n = 3$ cochleae/group; one way ANOVA, Ctrl vs. DSS $p = 0.0039$; FMT aUC vs. FMT rUC $p = 0.0001$) giving additional evidence of BLB alteration.

The intrastrial fluid–blood barrier also includes many pericytes and peri-vascular-resident macrophage-like melanocytes. Barriers without these cells lose TJ proteins, become leaky, and are associated with tissue edema. Thus, to confirm our hypothesis of altered BLB permeability, we also performed immunofluorescence and western blot experiments to evaluate the expression level of desmin, a marker of cochlear pericytes. The immunofluorescence analyses performed on *stria*

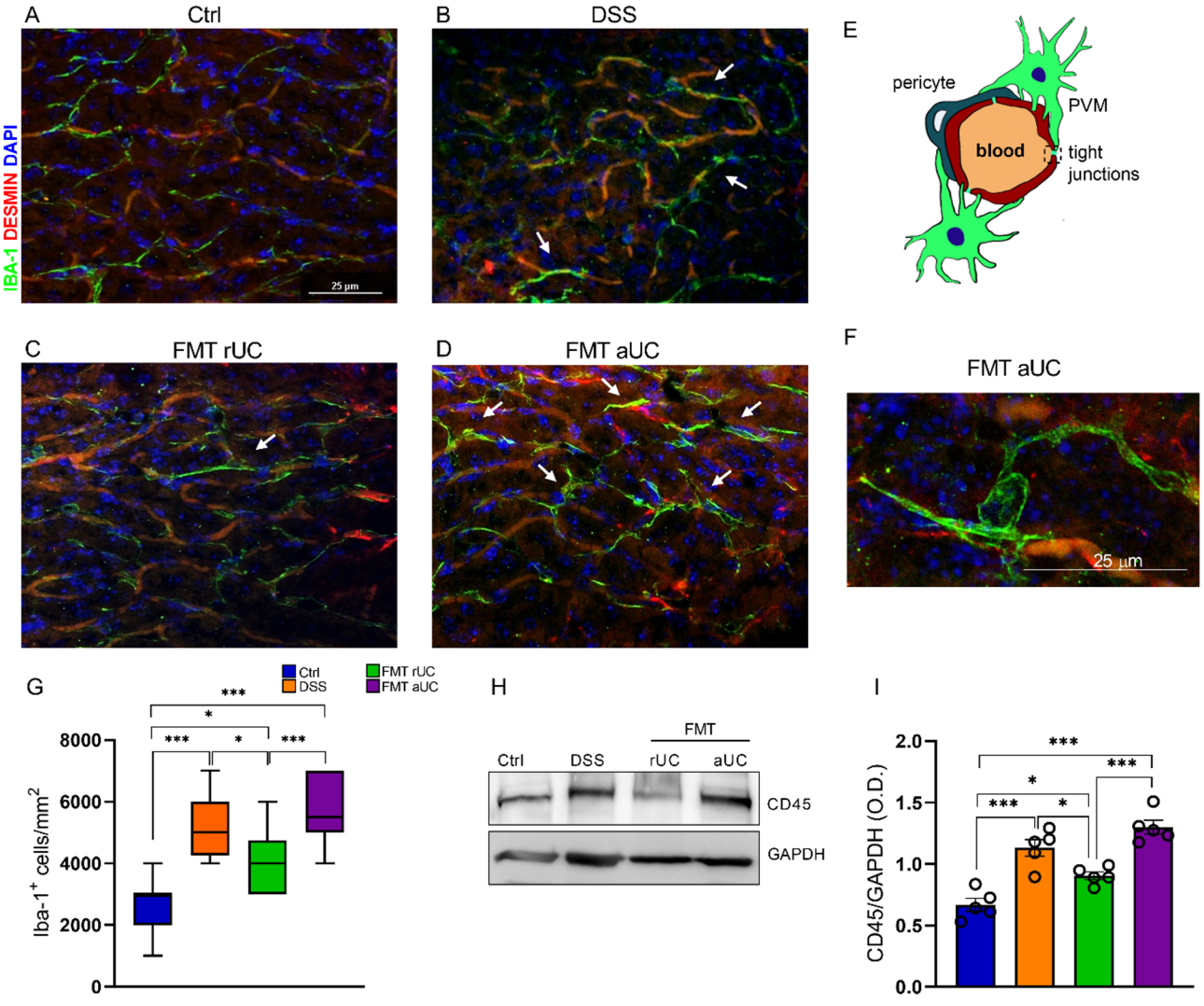


**Fig. 7** Cochlear damage associated with gut microbiota alteration involves macrophage/lymphocyte infiltration. **A-D**: Representative images of freshly explanted *stria vascularis* marked with IBA-1 (green fluorescence), desmin (red fluorescence) and stained with DAPI (blue fluorescence) to identify cell nuclei. Arrows indicate macrophages surrounding blood vessels **E**: Scheme illustrating perivascular macrophages (PVM) and pericytes around blood vessels. **F**: Representative confocal image (60×) of a PVM (green fluorescence) in the FMT aUC group. Scale bar: 25 µm. **G**: Histograms showing the number of IBA-1 positive cells in *stria vascularis* whole mount. **H**: Representative western blot images showing the expression of CD45 in all experimental groups. **I**: Bar graphs showing the results of densitometric analyses for CD45, normalized to total protein level (GAPDH). Data are expressed as mean ± SEM. Asterisks indicate significant differences among groups (*$p < 0.05$; ** $p < 0.01$; *** $p < 0.001$)

*vascularis* whole mount, show pericytes polygonal cell body with long, slender processes in control (Fig. 9A) and FMT rUC specimens (Fig. 9C).

In contrast, desmin labelling was very faint and discontinuous in DSS (Fig. 9B) and FMT aUC (Fig. 9D) *stria vascularis* samples. Western blot analyses in cochlear lysates confirmed immunofluorescence data, showing a significant reduction of desmin level in DSS and FMT aUC specimens with respect to Ctrl and FMT rUC specimens (Fig. 9I, J; $n = 3$ cochleae/group; one way ANOVA, Ctrl vs. DSS $p < 0.0001$; Ctrl vs. FMT aUC $p < 0.0001$; FMT rUC vs. FMT aUC $p = 0.0039$). Prompted by the presence of BLB structural alterations, we also studied vascular permeability by visualizing IgG extravasated around the vessels. Our immunofluorescence results showed a higher gradient of mouse IgG diffusing outside the vessel in DSS and FMT aUC groups (see arrows in Fig. 9F, H), whereas no signs of IgG extravasation were visible in Ctrl and FMT rUC groups (Fig. 9E, G).

Collectively, these data demonstrate an intrastriatal fluid–blood barrier damage or model of gut disease with altered intestinal permeability, caused by the altered expression of tight- and adherents-junction proteins, leading to loss of BLB integrity, extravasation, and, thus, increased pathogens permeability.

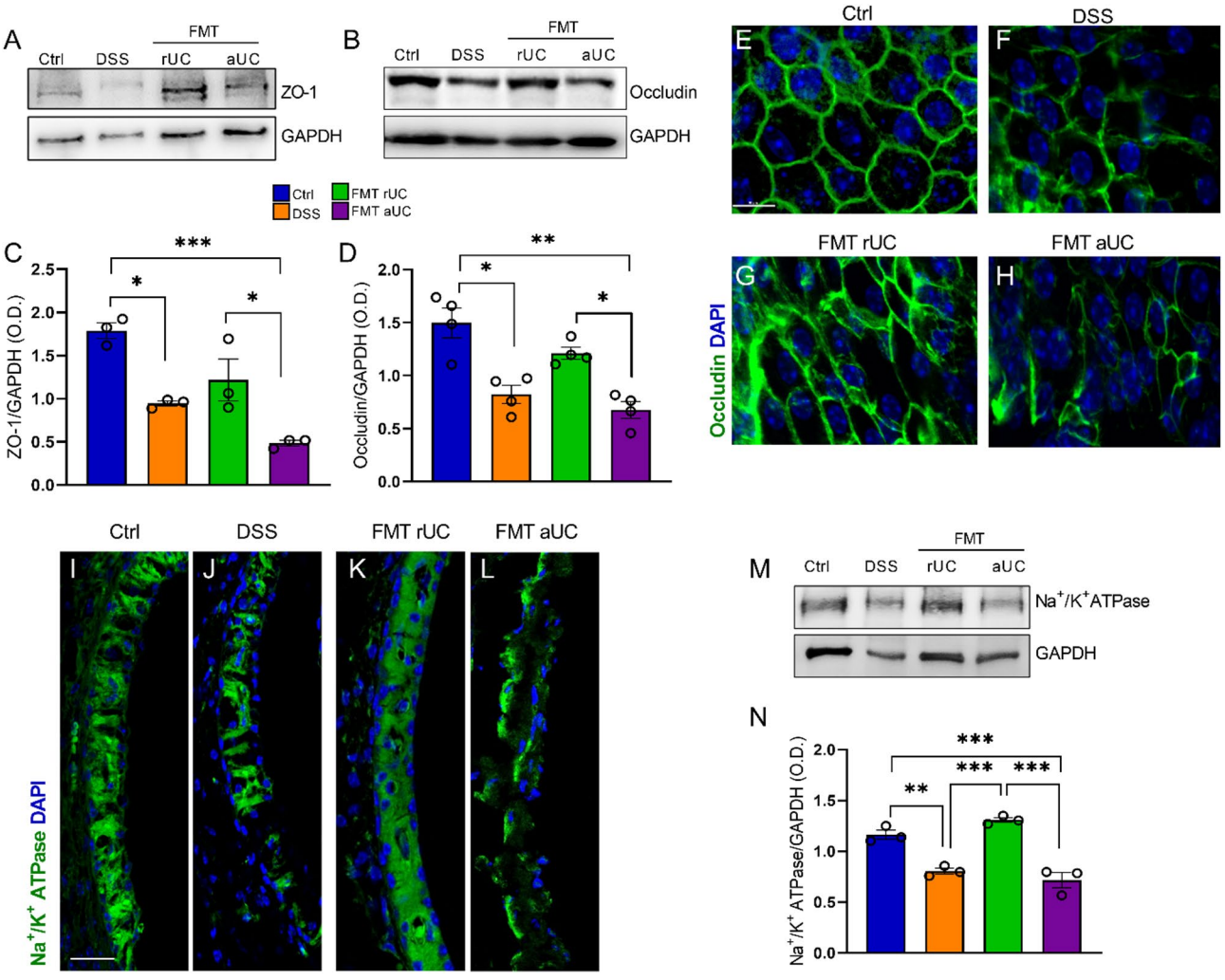


**Fig. 8** Gut microbiota state affects tight junctions and vascular integrity of *stria vascularis*. **A-D**: Representative western blot images showing ZO-1 (**A**) and occludin (**B**) levels in all experimental groups. **C-D**: Bar graphs representing results of densitometric analyses normalized to GAPDH. Data are expressed as mean ± SEM. **E-H**: Representative images of *stria vascularis* whole mount marked with occludin (green fluorescence) and stained with DAPI (blue fluorescence) to identify cell nuclei. Scale bar: 10 µm. **I-L**: Representative images of cochlear cryosections showing *stria vascularis* labeled with $Na^+/K^+$-ATPase (green fluorescence) and DAPI (blue fluorescence). Scale bar: 25 µm. **M**: Representative western blot images of $Na^+/K^+$-ATPase level in all experimental groups. **N**: Bar graphs (mean ± SEM) representing the densitometric analyses normalized to total protein level (GAPDH). Asterisks indicate significant differences among groups (*$p < 0.05$; **$p < 0.01$; ***$p < 0.001$)

## Discussion

In animal models, exposure to loud noise proved to cause gut microbiota alterations, host immune responses and long-lasting defects in glucose regulation. Moreover, noise exposure can affect the gut-brain axis, altering gut microbial community composition, disrupting the intestinal epithelial barrier, and accelerating age-related neuroinflammation, leading to an increased susceptibility to neurodegenerative processes in senescent mice [33].

Although several studies have suggested the existence of a gut-brain axis, no study has documented a connection between gut inflammation, gut microbiota alteration and the inner ear. Here, we collected experimental evidence demonstrating that gut inflammation and intestinal dysbiosis are associated with inner ear pathology. For this purpose, we used a well-known animal model of intestinal colitis caused by DSS [10–12, 24] together with a well-established modality of modulation of intestinal microbiota: FMT. DSS is able to arise colitis in mice causing a brick in the intestinal barrier, with an important traslocation of microbial products and abnormal immune activation [34]. DSS is also the main cause of gut microbiota changes, with an increase of relative abundances of Bacteriodetes and Proteobacteria, and a decrease of relative abundance of Firmicutes, Lactobacillus, Butyricicoccus, Lachnoclostridium, Olsenella and Odoribacter [35–37]. Most microbes in the Firmicutes phylum have anti-inflammatory functions by modulating

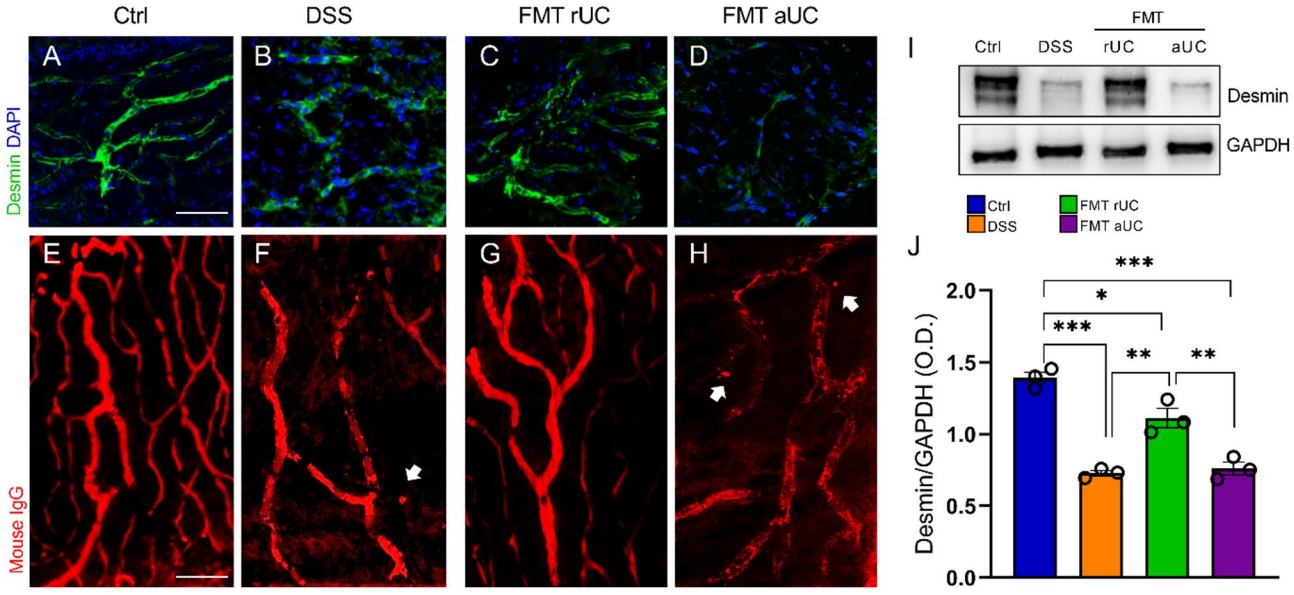


**Fig. 9** Cochlear vascular dysfunction and blood-labyrinth barrier increased permeability. **A-D**: Representative images of freshly explanted *stria vascularis* marked with desmin (green fluorescence) to visualize pericytes and stained with DAPI (blue fluorescence) to identify cell nuclei. **E-H**: Representative images of *stria vascularis* whole mount stained with Alexa Fluor 546 mouse IgG to visualize the capillary network. Arrows in **F** and **H** indicate mouse immunoglobulin fluorescence out of the vessels. Scale bar: 25 µm. **I**, **J**: Representative western blot images showing desmin expression level (**I**) and densitometric analysis (**J**) with respect to total protein level (GAPDH). Asterisks indicate significant differences among groups (*$p < 0.05$; **$p < 0.01$; ***$p < 0.001$)

colon pH which inhibits pathogen growth. They also produce *Short Chain Fatty Acids* (SCFAs) from non-digestible carbohydrates, that have important trophic functions for gut health, such as the reduction of oxidative status in the colon [38]. An increase in the population of microbes in the Bacteroidetes phylum is known to produce significantly high LPS levels which in turn regulate pro-inflammatory mediators through the NF-κB and AKT pathways in colonic macrophages [39, 40].

DSS induces in mice a disease that is very similar to UC in human. UC is inflammatory chronic conditions of the gastrointestinal tract, characterized by alternating periods of remission and active intestinal inflammation [41, 42]. During the active stage of the disease, UC is characterized by dysbiosis condition, i.e. a main imbalance between pro-inflammatory and anti-inflammatory phyla and genera [43]. This *dysbiosis* exacerbates immune dysfunction in UC [44, 45].

These findings explain what was observed also in our mice: the increase of pro-inflammatory cytokines and of histologic score also in mice treated with FMT aUC is due to higher relative abundance of *Bacteroides* and *Prevotella*, and lower abundance of *Lattobacillus*, *Fecalibacterium* and *Akkermansia*.

The choice of two different patient donor profiles, one more physiological like the rUC (confirmed also by α-diversity index in Fig. 3), and one more dysbiotic like aUC, allowed us to access the modulatory effect of gut microbiota composition on ear function. To investigate whether a reverse gut-ear axis exists, we first evaluated auditory function by recording ABRs and we found an increase in auditory threshold in mice with colitis induced by DSS and by FMT from aUC donors. To better understand the link between gut inflammation, gut microbiota alteration and inner ear impairment, we focused on the common hallmarks of intestinal inflammation and cochlear damage: oxidative stress and inflammation. Indeed, a pathological shift in gut bacteria is associated with an inflammatory response, leading to a state of chronic inflammation and oxidative stress [46]. Redox imbalance occurring during inflammation can amplify dysbiosis, affecting the microbial diversity in the gut and promoting the outgrowth of specific bacterial taxa [47]. Moreover, intestinal inflammation associated with leukocyte infiltration is linked to the generation of ROS. Interestingly, in the cochlea, we found high levels of ROS, protein nitrosylation, and lipid peroxidation along with decreased endogenous antioxidant defenses and increased inflammatory markers in mice exhibiting gut microbiota alterations (DSS and FMT aUC groups). This oxidative-inflammatory damage was partially counteracted by boosting overall gut diversity with FMT from rUC donors, suggesting an oxidative-inflammatory state of the gut-inner ear axis.

Cochlear oxidative stress can also induce the secretion of inflammatory cytokines (such as TNF-α and IL-1β) through NF-κB activation, a redox-sensitive transcription factor of crucial importance in inflammation. Indeed, the transcription of NF-κB-dependent genes has been shown to influence the levels of ROS, and in turn,

NF-κB activity is also affected by oxidative stress status [15]. In the cochleae of mice with gut dysbiosis, we also found altered levels of MyD88, one of the most important adaptor proteins in TLR signal transduction, activating downstream molecules such as NF-κB [48]. Several studies have shown the in vivo requirement of TLR signaling in mediating oxidative stress injury, and increasing evidence has shown that the activation of NOX isoforms is involved in the link between oxidative stress and TLR-dependent signaling pathways [49]. In addition, TLR response can trigger the secretion of pro-inflammatory markers, leading to a consequent increased expression of iNOS, and promoting the generation of NO [50]. Interestingly, we found an increased level of iNOS in the cochleae of mice with intestinal inflammation, thus providing experimental data supporting the hypothesis that oxidative stress/MyD88/NF-κB signaling triggers the upregulation of inflammatory markers in the cochlea of such mice.

Finally, we explored the hypothesis that, in our experimental model, the inflammatory markers released in the systemic circulation from the gut would affect BLB permeability, allowing the spread of macrophages and immune cells to the inner ear, leading to oxidative stress, inflammation and hearing impairment.

Previous studies have shown that gut microbiota can affect the permeability of the BBB, which is crucial to brain development and function. Interestingly, the structure regulating inner ear fluid homeostasis, the BLB, has a similar organization. BLB consists of several TJs and adherent junction proteins, including ZO-1, occludin, and VE-cadherin. Endothelial cells and pericytes that are integrated into the structure of the cochlear vessels are crucial components of the BLB, maintaining the integrity of the barrier between the blood and intrastrial space [51].

Gut-associated inflammatory factors, such as interferon-γ and pro-inflammatory cytokines, are responsible for breaking the integrity of the BBB when they enter the systemic circulation through the disruption of the gut mucosal barrier [52]. Therefore, we investigated a similar possible effect on the gut-cochlear axis. Our data showed a significant decrease in proteins with an essential role in the BLB structure, such as ZO-1 and occludin, together with signs of extravasation, altered pericyte structure, and leukocyte and macrophage infiltration, marked with CD45 and IBA-1 respectively, in the cochlea of mice with altered microbiota. These findings support the hypothesis of a direct impact of gut dysbiosis and disrupted intestinal barrier on BLB permeability.

It is known that the collapse of this barrier integrity causes a reduction in endocochlear potential, resulting from the continued active redistribution of $K^+$ ions from the endolymphatic space [53]. Notably, we also found signs of extravasation and altered $Na^+/K^+$-ATPase levels, playing a crucial role in maintaining the integrity of BLB and the endocochlear potential, suggesting not only BLB hyperpermeability but also possible functional damage of the *stria vascularis*, which is also supported by the morphological damage in type II fibrocyte density we observed in the lateral wall.

Collectively, we provided for the first time to our knowledge, experimental evidence supporting the impact of the intestinal inflammatory status on cochlear functions, with increased BLB permeability, macrophage and immune cell infiltration in cochlear structures, probably boosting oxidative stress/inflammatory pathway, leading to hearing impairment. Although our data provided for the first time experimental results of a link gut-cochlea, some limitations of the study regard the lack of direct evidence of cause-effect mechanisms of all morphological and molecular alterations we reported in the cochlea. Further studies are needed to support our hypothesis of the primary role of altered BLB permeability, leading to macrophage cochlear infiltration driving oxidative stress and inflammation. In summary, FMT rUC showed protective effects by improving DAI score, relieving colon pathological damages, and reducing cytokine expression. The effects of gut microbiota modulation were reflected far from the intestine, also in the cochlea: FMT intervention could increase SCFAs production by reducing oxidative status and by inhibiting the activation of the NF-κB signaling pathway.

Our data pave the way to further experimental studies exploring the complex relationship between gut dysbiosis and cochlear pathologies, with intriguing implications from a translational point of view.

## Supplementary Information

The online version contains supplementary material available at https://doi.org/10.1186/s12964-025-02338-1.

Supplementary Material 1

Supplementary Material 2

**Acknowledgements**

We would like to acknowledge the contribution of the Core Facility G-STeP "Electrophysiology", the contribution of the Core Facility G-STeP "Microscopy", Fondazione Policlinico Universitario "A.Gemelli" IRCCS. A special thanks to Fondazione Roma for the continuous and crucial support to our scientific research.

**Author contributions**

AP: experimental design, experimental procedures, data curation; VP: development of the experimental model, writing-original draft preparation; AP, VP, VMH, RM: investigation, methodology; FP: writing-original draft preparation, supervision; FDC, LP: data curation; CG, JG, MEC, GC, MT: resources; PP, LM, VE: writing-original draft preparation; GI, LRL: writing-review and editing; AG: funding acquisition; ARF and FS: conceptualization, supervision. All authors read and approved the final manuscript.

**Funding**
This article was supported by #NEXTGENERATIONEU (NGEU) and founded by the Ministry of University and Research (MUR), National Recovery and Resilience Plan (NRRP), project MNESYS (PE0000006)-A Multiscale integrated approach to the study of the nervous system in the health and disease (DN. 1553 11.10.2022). This study was financially supported by "Ricerca Corrente" from Fondazione Policlinico Universitario "A. Gemelli" IRCCS to C.G. Università Cattolica del Sacro Cuore contributed to the funding of this research project and its publication (D3.1 2024).

**Data availability**
No datasets were generated or analysed during the current study.

## Declarations

**Ethics approval and consent to participate**
All the experiments were approved by the local ethical committee and the Italian Ministry of Health. All animal procedures were conducted in accordance with the guidelines of our Institution and were approved by the ethical committee (n° 436/2017-PR, prot. 1F295.35.EXT.66). All efforts were made to reduce the number of animals and minimize their suffering in accordance with the European Community Council Directive of November 24, 1986(86/609/EEC).

**Consent for publication**
Not applicable.

**Competing interests**
The authors declare no competing interests.

**Author details**
[1]Dipartimento di Neuroscienze, Unità di Audiologia, Università degli Studi di Napoli Federico II, Naples 80131, Italy
[2]CeMAD Translational Research Laboratories Digestive Disease Center, Department of Medical and Surgical sciences, Fondazione Policlinico Universitario "A. Gemelli" IRCCS, Rome 00168, Italy
[3]Dipartimento di Neuroscienze, Università Cattolica del Sacro Cuore, Rome 00168, Italy
[4]Fondazione Policlinico Universitario A. Gemelli IRCCS, Rome 00168, Italy
[5]Dipartimento Testa-collo e organi di senso, Università Cattolica del Sacro Cuore, Rome 00168, Italy
[6]Immunologia, Reumatologia e Malattie Infettive, Unità di microbioma umano, IRCCS, Ospedale Pediatrico Bambino Gesù, Rome, Italy
[7]Unità di Microbiomica e Microbioma Umano, Ospedale Pediatrico Bambino Gesù IRCCS, Rome 00165, Italy
[8]Cen.Ri.S., Università Cattolica del Sacro Cuore, Rome 00168, Italy
[9]Digestive Disease Center "CeMAD", Internal Medicine and Gastroenterology, Fondazione Policlinico Universitario "A. Gemelli" IRCCS, Rome 00168, Italy
[10]Dipartimento di Medicina e Chirurgia Traslazionale, Università Cattolica del Sacro Cuore, Rome 00168, Italy
[11]Department of Life Science, Health, and Health Professions Link Campus University, Rome 00165, Italy

Received: 3 March 2025 / Accepted: 2 July 2025
Published online: 26 July 2025

**References**

1. Cryan JF, O'Riordan KJ, Cowan CSM, Sandhu KV, Bastiaanssen TFS, Boehme M, Codagnone MG, Cussotto S, Fulling C, Golubeva AV, et al. The Microbiota-Gut-Brain Axis. Physiol Rev. 2019;99(4):1877–2013.
2. Morais LH, Schreiber HL 4th, Mazmanian SK. The gut microbiota-brain axis in behaviour and brain disorders. Nat Rev Microbiol. 2021;19(4):241–55.
3. Martin JC, Chang C, Boschetti G, Ungaro R, Giri M, Grout JA, Gettler K, Chuang LS, Nayar S, Greenstein AJ, et al. Single-Cell analysis of crohn's disease lesions identifies a pathogenic cellular module associated with resistance to Anti-TNF therapy. Cell. 2019;178(6):1493–e150820.
4. Yoo JY, Groer M, Dutra SVO, Sarkar A, McSkimming DI. Gut microbiota and immune system interactions. Microorganisms. 2020;8(10):1587.
5. Pickard JM, Zeng MY, Caruso R, Núñez G. Gut microbiota: role in pathogen colonization, immune responses, and inflammatory disease. Immunol Rev. 2017;279(1):70–89.
6. Lin CH, Chen CC, Chiang HL, Liou JM, Chang CM, Lu TP, Chuang EY, Tai YC, Cheng C, Lin HY, et al. Altered gut microbiota and inflammatory cytokine responses in patients with parkinson's disease. J Neuroinflammation. 2019;16(1):129.
7. Li X, Yu M, Zhao Q, Yu Y. Prospective therapeutics for intestinal and hepatic fibrosis. Bioeng Transl Med. 2023;8(6):e10579.
8. Uyanik B, Grigorash BB, Goloudina AR, Demidov ON. DNA damage-induced phosphatase Wip1 in regulation of hematopoiesis, immune system and inflammation. Cell Death Discov. 2017;3:17018.
9. Wang L, Hu Y, Song B, Xiong Y, Wang J, Chen D. Targeting JAK/STAT signaling pathways in treatment of inflammatory bowel disease. Inflamm Res. 2021;70(7):753–64.
10. Wei W, Mu S, Han Y, Chen Y, Kuang Z, Wu X, Luo Y, Tong C, Zhang Y, Yang Y, Song Z. Gpr174 knockout alleviates DSS-Induced colitis via regulating the immune function of dendritic cells. Front Immunol. 2022;13:841254.
11. Nguepi Tsopmejio IS, Yuan J, Diao Z, Fan W, Wei J, Zhao C, Li Y, Song H. Auricularia polytricha and flammulina velutipes reduce liver injury in DSS-induced inflammatory bowel disease by improving inflammation, oxidative stress, and apoptosis through the regulation of TLR4/NF-κB signaling pathways. J Nutr Biochem. 2023;111:109190.
12. Yao L, Chen X, Shen M, Zhao Y, Cao Q. Isosteviol attenuates DSS-induced colitis by maintaining intestinal barrier function through PDK1/AKT/NF-κB signaling pathway. Int Immunopharmacol. 2023;114:109532.
13. Maguire M, Maguire G. Gut dysbiosis, leaky gut, and intestinal epithelial proliferation in neurological disorders: towards the development of a new therapeutic using amino acids, prebiotics, probiotics, and postbiotics. Rev Neurosci. 2019;30(2):179–201.
14. Takiishi T, Fenero CIM, Câmara NOS. Intestinal barrier and gut microbiota: shaping our immune responses throughout life. Tissue Barriers. 2017;5(4):e1373208.
15. Liu T, Zhang L, Joo D, Sun SC. NF-κB signaling in inflammation. Signal Transduct Target Ther. 2017;2:17023.
16. Fetoni AR, Paciello F, Rolesi R, Paludetti G, Troiani D. Targeting dysregulation of redox homeostasis in noise-induced hearing loss: oxidative stress and ROS signaling. Free Radic Biol Med. 2019;135:46–59.
17. Fetoni AR, Paciello F, Troiani D. Cisplatin chemotherapy and cochlear damage: otoprotective and chemosensitization properties of polyphenols. Antioxid Redox Signal. 2022;36(16–18):1229–45.
18. Paciello F, Pisani A, Rolesi R, Montuoro R, Mohamed-Hizam V, Boni G, Ripoli C, Galli J, Sisto R, Fetoni AR, Grassi C. Oxidative stress and inflammation cause auditory system damage via glial cell activation and dysregulated expression of gap junction proteins in an experimental model of styrene-induced oto/neurotoxicity. J Neuroinflammation. 2024;21(1):4.
19. Denton AJ, Godur DA, Mittal J, Bencie NB, Mittal R, Eshraghi AA. Recent advancements in Understanding the gut Microbiome and the inner ear Axis. Otolaryngol Clin North Am. 2022;55(5):1125–37.
20. Fousekis FS, Saridi M, Albani E, Daniel F, Katsanos KH, Kastanioudakis IG, Christodoulou DK. Ear involvement in inflammatory bowel disease: A review of the literature. J Clin Med Res. 2018;10(8):609–14.
21. Allen PW. Beethoven's triad: diarrhoea, deafness and cirrhosis (2022) A plausible solution to the 195-year-old controversy. Ann Diagn Pathol. 58:151904.
22. Bodh V, Kumar R, Sharma R, Sharma B, Sachdeva A, Azad R. Sensorineural hearing loss and ulcerative colitis in remission. Indian J Gastroenterol. 2022;41(2):143–8.
23. Bruce-Keller AJ, Salbaum JM, Luo M, Blanchard E 4th, Taylor CM, Welsh DA, Berthoud HR. Obese-type gut microbiota induce neurobehavioral changes in the absence of obesity. Biol Psychiatry. 2015;77(7):607–15.
24. Lopetuso LR, Petito V, Cufino V, Arena V, Stigliano E, Gerardi V, Gaetani E, Poscia A, Amato A, Cammarota G, et al. Locally injected Infliximab ameliorates murine DSS colitis: differences in serum and intestinal levels of drug between healthy and colitic mice. Dig Liver Dis. 2013;45(12):1017–21.
25. Maaser C, Sturm A, Vavricka SR, Kucharzik T, Fiorino G, Annese V, Calabrese E, Baumgart DC, Bettenworth D, Borralho Nunes P, Burisch J, Castiglione F, Eliakim R, Ellul P, González-Lama Y, Gordon H, Halligan S, Katsanos K, Kopylov U, Kotze PG, Krustinš E, Laghi A, Limdi JK, Rieder F, Rimola J, Taylor SA, Tolan D, van Rheenen P, Verstockt B, Stoker J. ECCO-ESGAR guideline for diagnostic assessment in IBD part 1: initial diagnosis, monitoring of known IBD, detection of complications. European crohn's and colitis organisation [ECCO] and

the European society of Gastrointestinal and abdominal radiology [ESGAR]. J Crohns Colitis. 2019;13(2):144–64. https://doi.org/10.1093/ecco-jcc/jjy113.
26. Romani L, Del Chierico F, Chiriaco M, Foligno S, Reddel S, Salvatori G, Cifaldi C, Faraci S, Finocchi A, Rossi P, et al. Gut mucosal and fecal microbiota profiling combined to intestinal immune system in neonates affected by intestinal ischemic injuries. Front Cell Infect Microbiol. 2020;10:59.
27. Caporaso JG, Kuczynski J, Stombaugh J, Bittinger K, Bushman FD, Costello EK, Fierer N, Peña AG, Goodrich JK, Gordon JI, et al. QIIME allows analysis of high-throughput community sequencing data. Nat Methods. 2010;7(5):335–6.
28. Edgar RC. Search and clustering orders of magnitude faster than BLAST. Bioinformatics. 2010;26(19):2460–1.
29. Fetoni AR, Eramo SL, Paciello F, Rolesi R, Samengo D, Paludetti G, Troiani D, Pani G. The redox protein p66(shc) mediates cochlear vascular dysfunction and transient noise-induced hearing loss. Sci Rep. 2016;6:25450.
30. Fetoni AR, Eramo SLM, Di Pino A, Rolesi R, Paciello F, Grassi C, Troiani D, Paludetti G. The antioxidant effect of Rosmarinic acid by different delivery routes in the animal model of Noise-Induced hearing loss. Otol Neurotol. 2018;39(3):378–86.
31. Paciello F, Zorzi V, Raspa M, Scavizzi F, Grassi C, Mammano F, Fetoni AR. Connexin 30 deletion exacerbates cochlear senescence and age-related hearing loss. Front Cell Dev Biol. 2022;10:950837.
32. Fetoni AR, Pisani A, Rolesi R, Paciello F, Viziano A, Moleti A, Sisto R, Troiani D, Paludetti G, Grassi C. Early Noise-Induced hearing loss accelerates presbycusis altering aging processes in the cochlea. Front Aging Neurosci. 2022;14:803973.
33. Cui B, Su D, Li W, She X, Zhang M, Wang R, Zhai Q. Effects of chronic noise exposure on the microbiome-gut-brain axis in senescence-accelerated prone mice: implications for alzheimer's disease. J Neuroinflammation. 2018;15(1):190.
34. Chang CS, Liao YC, Huang CT, Lin CM, Cheung CHY, Ruan JW, et al. Identification of a gut microbiota member that ameliorates DSS-induced colitis in intestinal barrier enhanced Dusp6-deficient mice. Cell Rep. 2021;37(8):110016.
35. Zhang W, Zou G, Li B, Du X, Sun Z, Sun Y, Jiang X. Fecal microbiota transplantation (FMT) alleviates experimental colitis in mice by gut microbiota regulation. J Microbiol Biotechnol. 2020;30(8):1132–41.
36. Clemente JC, Manasson J, Scher JU. The role of the gut Microbiome in systemic inflammatory disease. BMJ. 2018;360:j5145.
37. Sun MC, Zhang FC, Yin X, Cheng BJ, Zhao CH, Wang YL, Zhang ZZ, Hao HW, Zhang TH, Ye HQ. Lactobacillus reuteri F-9-35 prevents DSS-Induced colitis by inhibiting Proinflammatory gene expression and restoring the gut microbiota in mice. J Food Sci. 2018;83(10):2645–52.
38. Fusco W, Lorenzo MB, Cintoni M, Porcari S, Rinninella E, Kaitsas F, Lener E, Mele MC, Gasbarrini A, Collado MC, Cammarota G, Ianiro G. Short-Chain Fatty-Acid-Producing bacteria: key components of the human gut microbiota. Nutrients. 2023;15(9):2211.
39. Aderem A, Ulevitch RJ. Toll-like receptors in the induction of the innate immune response. Nature. 2000;406(6797):782–7.
40. Lamping N, Dettmer R, Schröder NW, Pfeil D, Hallatschek W, Burger R, Schumann RR. LPS-binding protein protects mice from septic shock caused by LPS or gram-negative bacteria. J Clin Invest. 1998;101(10):2065–71.
41. Danese S, Sans M, Fiocchi C. Inflammatory bowel disease: the role of environmental factors. Autoimmun Rev. 2004;3(5):394–400.
42. Le Berre C, Danese S, Peyrin-Biroulet L. Can we change the natural course of inflammatory bowel disease? Th Adv Gastroenterol. 2023;16:17562848231163118.
43. Lepage P, Häsler R, Spehlmann ME, Rehman A, Zvirbliene A, Begun A, Ott S, Kupcinskas L, Doré J, Raedler A, Schreiber S. Twin study indicates loss of interaction between microbiota and mucosa of patients with ulcerative colitis. Gastroenterology. 2011;141(1):227–36.
44. Burrello C, Garavaglia F, Cribiù FM, Ercoli G, Lopez G, Troisi J, Colucci A, Guglietta S, Carloni S, Guglielmetti S, Taverniti V, Nizzoli G, Bosari S, Caprioli F, Rescigno M, Facciotti F. Therapeutic faecal microbiota transplantation controls intestinal inflammation through IL10 secretion by immune cells. Nat Commun. 2018;9(1):5184.
45. Honda K, Littman DR. The microbiota in adaptive immune homeostasis and disease. Nature. 2016;535(7610):75–84.
46. Kunst C, Schmid S, Michalski M, Tümen D, Buttenschön J, Müller M, Gülow K. The influence of gut microbiota on oxidative stress and the immune system. Biomedicines. 2023;11(5):1388.
47. Weiss GA, Hennet T. Mechanisms and consequences of intestinal dysbiosis. Cell Mol Life Sci. 2017;74(16):2959–77.
48. Kuwabara WMT, Yokota CNF, Curi R, Alba-Loureiro TC. Obesity and type 2 diabetes mellitus induce lipopolysaccharide tolerance in rat neutrophils. Sci Rep. 2018;8(1):17534.
49. Gill R, Tsung A, Billiar T. Linking oxidative stress to inflammation: Toll-like receptors. Free Radic Biol Med. 2010;48(9):1121–32.
50. Lewis RS, Kolesnik TB, Kuang Z, D'Cruz AA, Blewitt ME, Masters SL, Low A, Willson T, Norton RS, Nicholson SE. TLR regulation of SPSB1 controls inducible nitric oxide synthase induction. J Immunol. 2011;187(7):3798–805.
51. Ito T, Kurata N, Fukunaga Y. Tissue-Resident macrophages in the stria vascularis. Front Neurol. 2022;13:818395.
52. Mou Y, Du Y, Zhou L, Yue J, Hu X, Liu Y, Chen S, Lin X, Zhang G, Xiao H, et al. Gut microbiota interact with the brain through systemic chronic inflammation: implications on neuroinflammation, neurodegeneration, and aging. Front Immunol. 2022;13:796288.
53. Ohlemiller KK, Dwyer N, Henson V, Fasman K, Hirose K. A critical evaluation of «leakage» at the cochlear blood-stria-barrier and its functional significance. Front Mol Neurosci. 2024;17:1368058.

## Publisher's note